Interaction of the Joining Region in Junctophilin-2 with the L-type Ca²⁺ Channel Is Pivotal for Cardiac Dyad Assembly and Intracellular Ca²⁺ Dynamics

Polina Gross[1], **Jaslyn Johnson**[1], **Carlos M. Romero**[1], **Deborah M. Eaton**[1], **Claire Poulet**[2], **Jose Sanchez-Alonso**[2], **Carla Lucarelli**[2], **Jean Ross**[3], **Andrew A. Gibb**[4], **Joanne F. Garbincius**[4], **Jonathan Lambert**[4], **Erdem Varol**[5], **Yijun Yang**[1], **Markus Wallner**[1,6,7], **Eric A. Feldsott**[1], **Hajime Kubo**[1], **Remus M. Berretta**[1], **Daohai Yu**[8], **Victor Rizzo**[1], **John Elrod**[4], **Abdelkarim Sabri**[1], **Julia Gorelik**[2], **Xiongwen Chen**[1], **Steven R. Houser**[1]

[1]Lewis Katz Temple University School of Medicine, Cardiovascular Research Center, Department of Physiology, Philadelphia

[2]Imperial College London, Department of Cardiovascular Sciences, Imperial Centre for Translational and Experimental Medicine, National Heart and Lung Institute, London

[3]Bioimaging Center Research, Delaware Biotechnology Institute, Newark

[4]Lewis Katz Temple University School of Medicine, Center for Translational Medicine, Department of Pharmacology, Philadelphia

[5]Columbia University, Center for Theoretical Neuroscience, Department of Statistics, New York, NY

[6]Medical University of Graz, Division of Cardiology, Graz, Austria

[7]Center for Biomarker Research in Medicine, CBmed GmbH, Graz, Austria

[8]Clinical Sciences, Lewis Katz School of Medicine, Temple University, Philadelphia.

Abstract

Rationale: Ca^{2+} induced Ca^{2+} release (CICR) in normal hearts requires close approximation of L-type calcium channels (LTCCs) within the transverse tubules (T-tubules), and Ryanodine receptors (RyR) within the junctional sarcoplasmic reticulum (jSR). CICR is disrupted in cardiac hypertrophy and heart failure, which is associated with loss of T-tubules and disruption of cardiac dyads. In these conditions, LTCCs are redistributed from the T-tubules to disrupt CICR. The molecular mechanism responsible for LTCCs recruitment to and from the T-tubules is not well known. Junctophilin-2 (JPH2) enables close association between T-tubules and the jSR to ensure efficient CICR. JPH2 has a so-called Joining region that is located near domains that interact with T-tubular plasma membrane, where LTCCs are housed. The idea that this Joining region directly interacts with LTCCs and contributes to LTCC recruitment to T-tubules is unknown.

Address correspondence to: Dr. Steven R. Houser, Lewis Katz School of Medicine, Temple University, Cardiovascular Research Center, 3500 N. Broad St. MERB 1080C, Philadelphia, PA 19140, srhouser@temple.edu.

DISCLOSURES

None.

Objective: To determine if the Joining region in JPH2 recruits LTCCs to T-tubules through direct molecular interaction in cardiomyocytes to enable efficient CICR.

Methods and Results: Modified abundance of JPH2 and redistribution of LTCC were studied in left ventricular hypertrophy *in vivo* and in cultured adult Feline and rat ventricular myocytes. Protein-protein interaction studies showed that the Joining region in JPH2 interacts with LTCC-α1C subunit and causes LTCCs distribution to the dyads, where they colocalize with RyRs. A JPH2 with induced mutations in the Joining region (mut^{PG1}JPH2) caused T-tubule remodeling and dyad loss, showing that an interaction between LTCC and JPH2 is crucial for T-tubule stabilization. mut^{PG1}JPH2 caused asynchronous Ca^{2+}-release with impaired excitation-contraction (EC) coupling after β-adrenergic stimulation. The disturbed Ca^{2+} regulation in mut^{PG1}JPH2 overexpressing myocytes caused Calcium/calmodulin-dependent kinase-II activation and altered myocyte bioenergetics.

Conclusions: The interaction between LTCC and the Joining region in JPH2 facilitates dyad assembly and maintains normal CIRC in cardiomyocytes.

Graphical Abstract
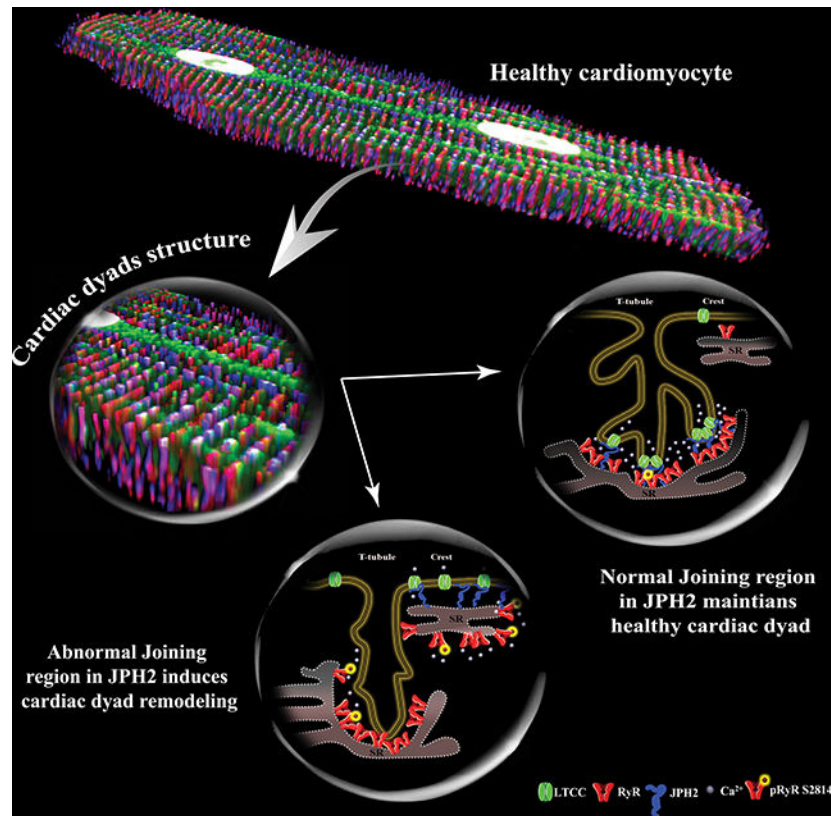
Keywords

Junctophilin-2; T-tubules; L-type calcium channels; calcium; dyad; arrhythmia; calcium regulation; excitation-contraction coupling; cardiac remodeling

Subject Terms:

Arrhythmias; Electrophysiology; Heart Failure; Ion Channels/Membrane Transport; Physiology

INTRODUCTION

Cardiovascular diseases can induce abnormalities in cardiac excitation-contraction (EC) coupling that include remodeling of the transverse tubule (T-tubule) system. These changes contribute to the altered contractile phenotype in heart failure (HF)[1–6]. T-tubules in ventricular cardiomyocyte form continuous plasma membrane (PM) invaginations from cell surface to the interior of the cells, coming into close proximity to the junctional sarcoplasmic reticulum (jSR), where contractile $[Ca^{2+}]$ is stored. This allows membrane excitation to be transmitted rapidly to the core of the myocyte, to induce a coordinated contraction. The architecture of T-tubules is composed of transverse and longitudinal elements, with variable lumen diameters and subdomains, which altogether form a dynamic system that can adjust to pathological stress[2, 6, 7]. Previous studies in humans and animal models have shown that hypertrophic and/or failing ventricular cardiomyocytes are associated with T-tubule remodeling, inhibition of *de novo* formation and a looser T-tubular network structure[6, 8–11].

L-Type Ca^{2+} channels (LTCCs) in T-tubules come into a close proximity with Ryanodine receptors (RyR) in the membrane of the jSR, at dyads, where they synchronize Ca^{2+} release. The maintenance of the dyad structure is regulated by multiple scaffolding proteins[11], among which Junctophilin-2 (JPH2) is central[12–14]. JPH2 is the cardiac isoform of the Junctophilins family that stabilizes the cardiac dyads by maintaining a precise space of 12–15nm between T-tubule and jSR membranes[15]. A transmembrane (TM) domain on the C terminus is responsible for anchoring JPH2 into the jSR membrane[12, 13]. The critical distance between T-tubule and jSR membranes is determined by the JPH2 α-helical domain. Attachment of JPH2 to the T-tubule surface membrane is mediated by multiple membrane occupation and recognition nexus (MORN) motifs on the N-terminus. These MORN motifs are interrupted by a Joining region, which has unknown function[13].

Knock out of cardiac JPH2 results in embryonic lethality, disorganized T-tubules and abnormal Ca^{2+} handling. JPH2 knock-down results in reduced Ca^{2+} transients, increased Ca^{2+} sparks and cellular hypertrophy, rapidly leading to HF[16–19]. Cardiac specific JPH2 overexpression mice had increased dyad frequency and attenuated progression from hypertrophy to HF[20]. Recent studies suggest that downregulation of JPH2 protein expression and mutations in JPH2 induce dilated and hypertrophic cardiomyopathies with arrhythmias in both humans[18, 21, 22] and murine models[21, 23]. Collectively these data suggest that JPH2 is crucial for T-tubular organization and synchronous Ca^{2+} release during EC coupling. Proper geometric dyad assembly enables close spatial proximity of LTCCs in the T-tubule to the juxtaposed RyRs in the jSR (~1:10 ratio)[24], which is essential for efficient EC coupling[25, 26]. Defective EC coupling has been found in hypertrophy and HF[27], leading to a reduction in Ca^{2+} transient amplitude, decreased SR Ca^{2+} content, asynchronous SR Ca^{2+}

release, upregulation in Calcium/calmodulin-dependent kinase II (CaMKII) activity and mitochondrial bioenergetic decline [9, 15, 27–31].

The idea that disorganization of LTCCs within EC coupling domains contributes to abnormal EC coupling in disease has not been well studied. Previous studies largely examined LTCC density and showed either no substantial changes in the magnitude of the LTCC current ($I_{Ca,L}$) in HF[32, 33], or small decreases in LTCC density with preserved basal $I_{Ca,L}$ with increased adrenergic regulation[10, 34]. Our hypothesis is that T-tubular remodeling causes disruption of LTCC targeting to dyads to disrupt EC coupling. The short life span of functional LTCC[35, 36] requires a well-regulated dynamic process of LTCC synthesis, trafficking, recycling and degradation in cardiomyocytes. Moreover, the necessity to preserve a functional pool of LTCCs in the dyads, at any given time, suggests that intracellular LTCC reservoirs can be mobilized in and out of distinct PM subdomains[2] in the cardiomyocyte. Some recent studies suggest that HF leads to a redistribution of LTCC away from the T-tubules[37, 38], decreased LTCC density in the T-tubules and increased $I_{Ca,L}$ density at the cell surface[39]. The mechanisms by which the LTCC is targeted to the T-tubules is not fully understood but could involve LTCC β2a subunit[40] and scaffolding protein BIN1[41] in the LTCC α1C trafficking. Recently, protein-protein interaction between LTCCs and junctophilins was identified in the triads of skeletal muscle. This interaction facilitated LTCC recruitment to the junctional membrane to ensure efficient skeletal muscle contraction[42, 43]. Similar LTCC-JPH2 interaction supported by caveolin-3 was recently reported in isolated cardiomyocytes[44]. The goal of the present study was to test the hypothesis that under physiological conditions, the Joining region in JPH2 holds LTCCs to dyads within T-tubules, and during hypertrophic remodeling, this interaction promotes LTCC displacement and redistribution away from T-tubules as JPH2 moves to other membrane locations. The current experiments show that JPH2 expression and T-tubule density and organization are reduced in a well-established Feline model of left ventricular hypertrophy (LVH) with EC coupling abnormalities[34, 45, 46]. We also used primary cultures of isolated adult feline ventricular myocytes (AFVMs) to explore the role of JPH2 in the time dependent loss of T-tubules in this preparation. Many studies have found that *in vitro* cultured adult cardiomyocytes undergo T-tubule remodeling that is reminiscent of de-differentiation[47–53].

To test our hypotheses, cultured AFVMs were infected with adenoviral (Ad) vectors carrying wild type (WT) JPH2 or JPH2 with a seven-point mutation in the JPH2 Joining region (mut[PG1]JPH2). WT JPH2 expression rescued T-tubule remodeling in cultured AFVM while mut[PG1]JPH2 promoted loss of T-tubules and localized JPH2 to the PM surface. These data suggest that the Joining region in JPH2 physically interacts with LTCC and enables LTCC specific recruitment to dyads to promote normal Ca^{2+} induced Ca^{2+} release (CICR). Also, these data indicate that disruption of EC coupling in disease involves the movement of JPH2 and the associated LTCCs from dyads to PM surface locations.

METHODS

Data Availability.

The data, methods used in the analysis (eg, program code or scripts for statistical packages), and materials used to conduct the research will be made available to any researcher for purposes of reproducing the results.

See the extended Materials and Methods section in the Online Data Supplement.

In brief, WT-JPH2 and mut[PG1]JPH2 adenoviral constructs were generated. Immunostaining, subcellular fractionation and PM sucrose density gradients were performed on cardiac tissue samples of LVH feline model. Adult rat and feline myocytes (ARVMs and AFVMS, respectively) were isolated. JPH2 immunostaining, Di-8-ANEPPS staining for T-tubules, PM sucrose density gradients and transmission electron microscopy were performed in ARVMs and/or AFVMs subjected to adenoviral-mediated expression of WT-JPH2 or mut[PG1]JPH2. Immunoprecipitation and proximity ligation assay were used to study protein-protein interaction between LTCC and JPH2. Cytosolic Ca^{2+} transients, confocal line scanning and caffeine-induced SR Ca^{2+} release were performed on paced myocytes loaded with Fluo-4AM. LTCC mediated Ca^{2+} currents were measured in AFVMs and ARVMs overexpressing WT-JPH2 or mut[PG1]JPH2 using standard patch clamping and Super resolution scanning patch clamp. Western blot analysis was used to evaluate expression levels of Ca^{2+} handling proteins in myocytes. Oxygen consumption assays were used to measure bioenergetics in AFVMs overexpressing WT-JPH2 or mut[PG1]JPH2. All Animal procedures were approved by the Temple University Institutional Animal Care and Use Committee, and in accordance with the United Kingdom Home Office Animals (Scientific Procedures) Act 1986 Amendment Regulations 2012, incorporating the EU Directive 2010/63/EU. Investigators were blinded as to the type of animal being studied, in all aspects of this study.

RESULTS

LVH decreases JPH2 expression on the plasma membrane and JPH2 and LTCC are redistributed across the sarcolemma.

Slow progressive pressure overload, via aortic constriction in Feline hearts, led to left ventricular (LV) hypertrophy with preserved fractional shortening (Figure 1A–D and Online Figure IA–B). Because compensated hypertrophy precedes development of HF, and since an impairment of T-tubule integrity (a function of regularity and density) begins before overt LV systolic dysfunction[1], we examined the effects of *in vivo* pressure overload induced cardiac hypertrophy on JPH2 protein expression and localization. The total protein abundance of JPH2 and LTCC were unchanged in hypertrophic and sham hearts (Figure 1E–G). Next, the LV cardiac tissue was separated into subcellular fractions (Online Figure ID) to examine the JPH2 and LTCC expression in the membrane fraction, as an indication for the T-tubular component. LVH induced significant reduction of JPH2 protein abundance only in the PM fractions (Figure 1E, H–I) and ~2-fold decrease in the ratio of JPH2 to LTCC pore-forming subunit α1C (Figure 1L). These changes were consistent with the molecular rearrangement of JPH2 across the PM, along with the remodeling of dyads and T-tubules

(Figure 1M and Online Figure IE). Sham hearts displayed organized JPH2 staining patterns colocalized with LTCC, while LVH hearts showed a disorganized JPH2 staining (Figure 1M.1 vs. 1M.2 – indicated by arrows). In addition, JPH2 staining in LVH hearts revealed protein organization implying aggregate patterns (Figure 1M.2 and Online Figure IE, H–J). The distribution of JPH2 and LTCC in myocardial membrane domains was also examined by isopycnic ultracentrifugation. JPH2 was detected within PM fractions F6-F7 in sham hearts. In LVH, a broader redistribution of JPH2 was detected within PM fractions F6-F9, indicating a shift of the membrane domains where JPH2 resides (Figure 1N). Similarly, LVH was associated with redistribution of LTCC α1C subunit and LTCC β2a subunit across membrane microdomains (Figure 1N).

Isolated adult cardiomyocytes in culture undergo T-tubule remodeling and JPH2 downregulation.

T-tubule and JPH2 remodeling were also studied in cultured AFVMs. AFVMs resemble human cardiomyocyte electrophysiological and Ca^{2+} handling properties[50, 54, 55], and they can be maintained for long periods of time in culture[50, 56]. Concurrently, after a few days in culture, AFVMs displayed myofibrillar disorganization with increased contractile duration and prolongation of action potential[50]. These phenotypic shifts in myocyte structure and function are similar to those seen *in vivo* LVH and HF humans and animal models [46, 49, 50, 57]. T-tubular remodeling was studied in AFVMs by staining T-tubules with a voltage sensitive dye. After 4 days in primary culture AFVMs (D4C) showed reduced T-tubular density compared to freshly isolated AFVMs (D0) (Figure 2A.1–2, 2B and 2C – D0 vs. D4C). Although, total JPH2 protein expression was unchanged in D4C cardiomyocytes compared to D0 cardiomyocytes (Figure 2J), immunofluorescence staining of JPH2 and Z-stack confocal scanning (Online Figure III.A) detected decreases in JPH2 density and integrity in D4C AFVMs (Figure 2D.1–2 and Figures 2E–F – D0 vs. D4C). The overall organization of JPH2 was changed but not its total abundance. D4C AFVMs showed redistribution of JPH2, LTCC α1C and β2a subunits within PM domains (Figure 3G and Online Figure V). Decreases in myofilament organization (Online Figure IIIB.1 and IIIB.2), disruption of Z-lines ultrastructure and reduced numbers of dyads (Figure 2L.1–2) were also observed in cultured AFVMs.

Mutating the Joining region in JPH2 exacerbates T-tubules remodeling and reduces dyad frequency.

We generated a mutant form of JPH2 with random seven-point mutations in the Joining region of human JPH2 isoform (with the consideration that human JPH2 shares 89% protein identity with Felis catus JPH2) and inserted it into an Adenoviral (Ad) vector. The mutant JPH2 reagent (Ad-mut[PG1]JPH2) was tagged with the HA peptide on the JPH2 N-terminus to determine transduction efficiency in AFVMs (85% at Day 4). Ad-WT (human) JPH2 with a HA tag was also studied (Figure 2G–H). We modeled the putative protein secondary and tertiary structures[58, 59] of HA-WT-JPH2 and HA-mut[PG1]JPH2 to explore the steric structure of JPH2. Overall, WT-JPH2 3D model (P-value 1.37×10^{-05}) showed a similar structure to the 3D model of mut[PG1]JPH2 (P-value 2.29×10^{-05}) (Figure 2I). Mapping of the secondary protein structure detected that mutation E209A mildly increased the probability of α-helix structure (55.7% in WT-JPH2 vs. 64.5% in mut[PG1]JPH2), while the rest of the mutations did

not introduce any critical alterations (Online Figure II). The modeling studies suggests that the seven-point mutations in mut^{PG1}JPH2 caused tertiary conformational changes in the Joining region without affecting MORN motifs, α-helical domain, divergent and TM domains (Online Table I).

JPH2 and HA protein expression were measured in AFVMs 4 days after transduction with Ad-WT-JPH2 and Ad-mut^{PG1}JPH2 (Figure 2J). Overexpression of WT-JPH2 in AFVMs prevented/reversed the T-tubules remodeling in D4C cultured AFVMs (Figure 2A.3). The density of T-tubular elements was increased along with increased T-tubular integrity (Figures 2B–2C). Very few T-tubules were detected in AFVMs transduced with mut^{PG1}JPH2 (Figure 2A.4). The density of T-tubular elements and T-tubule integrity were significantly lower in mut^{PG1}JPH2 than in D4C and WT-JPH2 overexpressing cardiomyocytes (Figure 2B and 2C). JPH2 and HA staining revealed that overexpression of WT-JPH2 restored JPH2 density compared to D4C AFVMs and increased JPH2 integrity (Figures 2D.3, 2E–F and 2K) without fully reversing the remodeling. Overexpression of mut^{PG1}JPH2, however, induced JPH2 localization to PM surface (Figure 2K), leaving the mid-section of the cardiomyocyte largely devoid of JPH2 (Figure 2D.4–D.5), as shown across Z-stack confocal scanning (Online Figure III.A). As a result, JPH2 density and integrity (Figure 2E–2F) in mid-section of mut^{PG1}JPH2 cardiomyocytes were significantly reduced compared to D0 and WT-JPH2 overexpressing cardiomyocytes. Importantly, T-tubular pattern and morphology differ between species. Small animal (rodents) exhibit denser, deeper and narrower T-tubular network than large mammals in association with the difference in their heart rates[2, 7]. We tested the effects of Ad-WT-JPH2 and Ad-mut^{PG1}JPH2 on isolated adult rat ventricular myocytes (ARVMs), which showed similar effects on T-tubule and JPH2 expression patterns that were observed in AFVMs (Online Figure IV).

We also studied the effect of WT-JPH2 and mut^{PG1}JPH2 overexpression on cardiomyocyte structure, dyad frequency and dyad morphology using Transmission electron microscopy (Figure 2L, Online Figure VI). Myofilament disorganization is apparent in D4C cardiomyocytes compared to freshly isolated cardiomyocytes in D0. Myofilament disorganization was maintained/restored by overexpression of WT-JPH2. However, overexpression of mut^{PG1}JPH2 induced morphological abnormalities that further deranged myofilament disarray (Online Figure IIIB). WT-JPH2 overexpression in AFVMs increased the length of the dyads, which was measured as the length between T-tubule/jSR contacts (Online Figure VI). mut^{PG1}JPH2 overexpression in AFVMs reduced the dyad frequency in comparison to dyad frequency detected in WT-JPH2 overexpressing cells (Figure 2L.4 and 2M). Despite changes in dyad frequency, the dyad length remained unaffected (Online Figure VI).

The Joining region in JPH2 interacts with the LTCC α1C subunit and induces localization of LTCC to dyad microdomains where it colocalizes with RyR.

Our hypothesis is that the Joining region in JPH2 is a site of molecular interaction between JPH2 and LTCC in the dyad. To explore this further, we purified PMs from AFVMs that were transduced with Ad-WT-JPH2 or with Ad-mut^{PG1}JPH2. The HA peptide tag was used in co-immunoprecipitation (Co-IP) studies. These Co-IP studies (Figure 3A) show that the

LTCC α1C subunit, but not the β2a subunit, is complexed with JPH2 in the cardiomyocyte PM. Quantification of Co-IP experiments showed similar pull-down of HA and Co-IP of JPH2 (Figures 3B–3C) between WT-JPH2 and mut^{PG1}JPH2 overexpressing myocytes. However, mutating the Joining region in JPH2 weakened the interactions between the LTCC α1C pore-forming subunit and JPH2 (Figure 3D). This was further substantiated using a highly specific and sensitive approach of proximity ligation (PLA) assay in single cells. Overexpression of mut^{PG1}JPH2 in ARVMs strongly reduced the association between JPH2 and LTCC α1C, in comparison to cardiomyocytes overexpressing WT-JPH2 (Figures 3E and 3F). To determine if the protein-protein interaction between JPH2 and LTCC α1C determines LTCC recruitment to specific membrane domains, we fractionated PM preparations from WT-JPH and mut^{PG1}JPH2 overexpressed AFVMs (Figure 3G). WT-JPH2 overexpression in cultured cardiomyocytes largely restored JPH2 and LTCC α1C distribution back to the fractions (F6-F7) of the PM where they reside in freshly isolated myocytes. However, mut^{PG1}JPH2 overexpression caused redistribution of JPH2 across the membrane and promoted a profound displacement of LTCC α1C from its typical fractions F6-F7 to fractions F6-F11.

Co-localization of LTCC with RyR is crucial for CICR and EC coupling. We further examined the relationship between LTCC-JPH2-RyR dyadic complexes in our AFVMs infected with WT or mutated JPH2. We immunolabeled LTCC, JPH2 and RyR and performed co-localization profiling using a distance-based approaches (see online methods). Freshly isolated AFVMs (D0) showed clear co-localization patterns of immunostained LTCC-JPH2-RyR (Online Figure VIIA.1) and LTCC-RyR (Figure 3H.1) dyadic complexes. These patterns were decreased in D4C AFVMs (Online Figure VIIA.2 and Figure 3H.2). In cardiomyocytes expressing WT-JPH2 co-localization of LTCC-JPH2-RyR and LTCC-RyR was preserved (Online Figure VIIA.3 and Figure 3H.3), even though, these cardiomyocytes still exhibited some structural remodeling (in comparison to D0 cardiomyocytes). In mut^{PG1}JPH2 overexpressing cardiomyocytes, immunostaining showed JPH2 localization to the surface sarcolemma with robustly reduced co-localization patterns of LTCC-JPH2-RyR (Online Figure VIIA.4) and LTCC-RyR complexes (Figure 3H.4). Quantitative analysis of LTCC-RyR co-localization (Figure 3I and Online Figure VIIF) and LTCC-JPH2 co-localization (Online Figures VIIB and VIIE) verified our qualitative findings. To determine if WT or mutated JPH2 constructs had any effect on LTCC expression, we measured LTCC density and integrity in the same set of images (Online Figure VIIC and VIID). We found that in all cultured AFVMs (baseline and transduced cells), LTCC integrity was reduced in comparison to D0 AFVMs. The density of LTCC was reduced in mut^{PG1}JPH2 transduced cells in comparison to D0 cells but not relatively to WT-JPH2 transduced cells. These changes are attributed to the cell remodeling in culture rather than to the mutated Joining region in JPH2. LTCC immunostaining controls are shown in Online Figure VIIG.

We next sought to distinguish whether JPH2 overexpression is sufficient to preserve the T-tubular system in cultured AFVMs, or the actual crosstalk between JPH2 and LTCC is crucial for the stabilization of T-tubules. LTCC (α1C) abundance in AFVMs was reduced by transducing cells with Ad-LTCC (α1C)-shRNA-V3 (Online Figure VIII). Staining of LTCC α1C supported reductions in the protein levels (Figure 4A – upper panel). Knocking down LTCC α1C did not result in further downregulation of JPH2 and T-tubule density and/or

integrity in culture, as shown in Ad-scramble shRNA control cells (Figure 4A – middle and lower panel, Figure 4B–E). Overexpression of both Ad-LTCC (α1C)-shRNA-V3 and Ad-WT-JPH2, induced increases in JPH2 levels with localization to the PM surface (Figure 4A – middle panel). JPH2 density and integrity were indeed restored in these cells (Figure 4B–C). However, the T-tubular network was not reestablished, as T-tubule density remained decreased (Figure 4D–E). Thus, it is likely that overexpression of JPH2 alone, without establishing LTCC-JPH2 interaction, is not sufficient to restore and stabilize T-tubules.

Disrupting the interaction between the Joining region in JPH2 and LTCC in cardiomyocytes impairs EC coupling and CICR.

The effect of modulating the interaction between the Joining region in JPH2 and the LTCC on cell physiology was explored by measuring cytosolic Ca^{2+} transients in AFVMs overexpressing either red fluorescence protein (RFP; control), WT-JPH2 or mut[PG1]JPH2. Given that β-adrenergic stimulation modulates intracellular Ca^{2+} release during EC coupling[60, 61], responses to the β-adrenergic agonist Isoproterenol (Iso 100nM) were also measured (Figure 5). Baseline Ca^{2+} transients were not different in any of the three groups. Iso induced similar increases in cytosolic Ca^{2+} transient amplitude in RFP and WT-JPH2 overexpressing myocytes. However, Iso did not significantly increase the amplitude of the Ca^{2+} transient in mut[PG1]JPH2 expressing AFVMs (Figure 5C–D), which was similarly observed also in LVH isolated myocytes (Online Figure IC). Iso accelerated the kinetics of Ca^{2+} transient decay in all groups (Figure 5E–G). The time to 90% recovery in WT-JPH2 overexpressed myocytes was longer after Iso (Figure 5G). Iso triggered pro-arrhythmic Ca^{2+} waves in mut[PG1]JPH2 AFVMs. Spontaneous Ca^{2+} release was observed between paced Ca^{2+} transients in the mut[PG1]JPH2 AFVMs (Figure 5H – indicated by arrows). This observation was similar to Ca^{2+} transients detected in isolated LVH cardiomyocytes (Online Figure IC). To better understand the mechanism of pro-arrhythmic Ca^{2+} transients in mut[PG1]JPH2 AFVMs, the spatial uniformity of SR Ca^{2+} release was examined with confocal line scanning (Figure 5I). At baseline, disordered Ca^{2+} wave propagation (>210msec) was observed in mut[PG1]JPH2 AFVMs. Spatial uniformity was significantly delayed in mut[PG1]JPH2 AFVMs compared to RFP and WT-JPH2 myocytes. Iso decreased the percentage of unresponsive Ca^{2+} release zones (likely couplons) in all groups. With Iso present, the spatial synchrony of couplons in mut[PG1]JPH2 myocytes still occurred significantly later than in WT-JPH2, or with a relative delay compared to RFP myocytes (Figure 5J). These results suggest that mut[PG1]JPH2 myocytes had fewer couplons than other myocytes, which is likely linked to the loss of T-tubules as well as to unresponsive couplons. Spontaneous Ca^{2+} release after slow pacing (Figure 5K) and faster pacing (Online Figure IXA) frequencies was observed in the presence of Iso mut[PG1]JPH2 infected myocytes. RFP and WT-JPH2 infected AFVMs exhibited synchronous Ca^{2+} release during 0.5Hz and 1Hz pacing. Spontaneous Ca^{2+} release events are typically attributed to pacing induced SR Ca^{2+} overload. mut[PG1]JPH2 expressing myocytes exhibited significant asynchronous Ca^{2+} release during pacing protocols. A distinct pattern of spontaneous Ca^{2+} release was observed during the pacing in these cells. In these myocytes local, submembrane Ca^{2+} release was observed at the edges of the cell and there was failure to propagate the Ca^{2+} wave either inward or along the myocyte (Figure 5K – indicated via black arrows). 3D plotting of the line scan images clearly showed that these spontaneous Ca^{2+} release events arose from the edges of

the mut^{PG1}JPH2 expressing cell (Figure 5L – indicated via black arrows). Following the pacing phase, mut^{PG1}JPH2 myocytes demonstrated multiple Ca^{2+}spontaneous releases, random Ca^{2+} triggered events (Figure 5K – black arrows) and Ca^{2+} alternans (Figure 5K – grey arrows). Using 3D plotting, we determined that spontaneous Ca^{2+} releases and Ca^{2+} alternans had uniform distribution across the cells, albeit with distinct intensities (Figure 5L – red arrows vs. grey arrows, respectively). These results suggest that SR Ca^{2+} uptake and release were altered in mut^{PG1}JPH2 myocytes. We found that Ca^{2+} alternans were abolished in the presence of CaMKII inhibitor – KN93 in mut^{PG1}JPH2 overexpressing myocytes (Online Figure IXB).

To determine if mutating the Joining region in JPH2 affected LTCC activity after Iso stimulation, we measured $I_{Ca,L}$ in single isolated AFVM overexpressing RFP, WT-JPH2 or mut^{PG1}JPH2. Basal peak $I_{Ca,L}$ density (Figure 6A) was not significantly different in any of the three groups. All groups also had substantial increase in $I_{Ca,L}$ after Iso (Figure 6A–B). There was a significant rightward shift in the voltage dependence of $I_{Ca,L}$ activation in the basal state of mut^{PG1}JPH2 myocytes compared to RFP and WT-JPH2 myocytes (Figure 6C). Iso induced the voltage dependence of $I_{Ca,L}$ activation to shift towards negative potentials in RFP and mut^{PG1}JPH2 myocytes without strongly affecting WT-JPH2 myocytes (Online Figure XA–C). A left shift in the voltage dependence of $I_{Ca,L}$ activation is typically observed with PKA-mediated phosphorylation of the LTCC complex with activation of β-adrenergic signaling[34, 60]. However, WT-JPH2 and mut^{PG1}JPH2 overexpressed myocytes still showed a shift of ~10mV towards more positive potentials relative to RFP control myocytes under Iso stimulation (Figure 6D), indicating aberrant regulation of LTCCs in these myocytes.

Super-resolution patch-clamp[62] was then used to determine LTCC function in specific PM microdomains in ARVMs overexpressed with Ad-WT-JPH2 or Ad- mut^{PG1}JPH2 (Figure 6E–G). Freshly isolated ARVMs exhibited a higher number of functional LTCCs per μm^2 in the T-tubules regions versus membrane surface (crest) (T-tubules>crest) (Figure 6F). This ratio was reversed after 4 days in primary culture in control cells (T-tubules<crest). Overexpression of WT-JPH2 in ARVM increased the density of functional LTCCs and restored the ratio of T-tubules>crest. Functional LTCCs were not detected in T-tubules of mut^{PG1}JPH2 overexpressing ARVMs. These results indicate that functional LTCCs were localized in the crest of mut^{PG1}JPH2 cells (Figure 6F). The LTCC open probability was also measured in the presence of LTCC agonist BayK8644 to ensure the maximal open probability of LTCCs (Figure 6G). The open probability of LTCCs was similar in all groups under these conditions, including LTCCs in the crest of mut^{PG1}JPH2 overexpressed cells.

To measure SR Ca^{2+} content, AFVMs were paced to a steady state and SR Ca^{2+} release was induced by a rapid application of caffeine. Similar amplitudes of caffeine-induced SR Ca^{2+} release was seen in the RFP, WT-JPH2 and mut^{PG1}JPH2 overexpressing AFVMs. Perfusing myocytes with Iso induced increase in SR Ca^{2+} release in RFP control and WT-JPH2 myocytes. However, an increase in the caffeine-induced SR Ca^{2+} release was not seen in mut^{PG1}JPH2 myocytes after Iso application, consistent with the lack of effects of Iso on the peak Ca^{2+} transient in these cells (Figure 6H–I). The Ca^{2+} clearance after caffeine-induced SR Ca^{2+} release was not different between the different groups (Figure 6J).

The effect of mut^{PG1}JPH2 overexpression on EC coupling proteins and Ca^{2+} handling proteins in cardiomyocytes.

JPH2 is an essential structural regulator of the dyadic cleft. Mutations in the Joining region of JPH2 resulted in changes in the dyad density and alterations of Ca^{2+} regulation in AFVMs. Overexpression of mut^{PG1}JPH2 in cardiomyocytes did not induce changes in the abundance levels of the EC coupling proteins residing in the cardiac dyads (Figure 7A–I and Online Figure XIA–E). No significant differences in the expression levels of total RyR, LTCC (α1C), sarcoplasmic reticulum calcium ATPase 2a (SERCA2a), Sodium-Calcium exchanger (NCX) or phospholamban (PLB) were observed. BIN1, which has been previously shown to localize to T-tubules and regulate LTCC trafficking to the T-tubules[41, 63], also did not differ in WT-JPH2 or mut^{PG1}JPH2 overexpressed AFVMs in comparison to D0 and D4C AFVMs. However, Calcium/calmodulin-dependent kinase II (CaMKII) activation in mut^{PG1}JPH2 myocytes was likely altered through autophosphorylation at Thr287 site[64] (Figure 7E). mut^{PG1}JPH2 myocytes exhibited increased RyR S2814 and PLB T17 phosphorylation (Figure 7C and 7H), which are known CaMKII phosphorylation sites[65, 66]. Phosphorylation sites of RyR S2808 and PLB S16 that are PKA mediated remained unaffected in mut^{PG1}JPH2 overexpressing myocytes (Figure 7B and 7G). These results suggest that mut^{PG1}JPH2 disrupts myocyte Ca^{2+} regulation leading to activation of CaMKII (at Thr287) and subsequent phosphorylation of critical SR Ca^{2+} handling proteins.

Cardiomyocyte overexpression of WT and mut^{PG1} JPH2 alter mitochondrial morphogenesis and bioenergetics.

Primary culture of AFVMS and mutations of the Joining region of JPH2 lead to disruption of Ca^{2+} homeostasis that could affect the energetic balance of the cell. We observed modified mitochondrial ultrastructure in myocytes overexpressing WT-JPH2 and mut^{PG1}JPH2. Using transmission electron microscopy, healthy D0 myocytes were visualized with cylindrical shaped mitochondria and rounded edges (and few round-shape mitochondria) that were highly organized in longitudinal rows (Figure 7J and Figure 2L.1). Remodeling of cardiomyocytes in cell culture resulted in a significant reduction of mitochondria number, accompanied by enhanced shape variability (Figure 7K, 7N and Figure 2L.2). Overall, the average mitochondrial surface area was increased in D4C myocytes (Figure 7O). This increase also occurred in WT-JPH2 overexpressing myocytes, with a reduction in mitochondrial circularity (Figure 7L, Figure 2L.3 and Figure 7P). mut^{PG1}JPH2 overexpressing myocytes exhibited a significant reduction in mitochondrial number (Figure 7N) compared to all other conditions. In addition, the mitochondria in these cells appeared more tubular with an increase in aspect ratio and 2-fold larger than mitochondria in D4C or WT-JPH2 myocytes (Figures 7M, 7O, 7Q and Figure 2L.4). In freshly isolated myocytes, the mitochondrial distribution is mostly spacious with occasional events of physical contacts between two adjacent mitochondria, termed as "kissing" junctions[67, 68], which were also present in D4C and mut^{PG1}JPH2 myocytes. However, WT-JPH2 myocytes demonstrated significantly increased frequency of "kissing" junctions (Online Table II and Figure 7J–M indicated in yellow arrows), suggesting coordinated communication through structural associations. Other conserved structures known as mitochondrial nanotunnels[68, 69] were detected in electron microscopy images. Nanotunnels

were positively identified if they clearly contained the outer and inner mitochondrial membranes along with a continuation of mitochondrial matrix and cristae. We quantified the frequency of short distance nanotunnels (<1μm) and long distance nanotunnels (1μm) (Figure 7K and Figure 7J, respectively – indicated between red arrows), and found that nanotunnels are relatively rare in D0 myocytes (Online Table II). D4C and WT-JPH2 myocytes showed a higher abundance of nanotunnel structures, with a mainly short length nanotunnels being observed. Conversely, mut[PG1]JPH2 myocytes showed significantly increased frequency in long distance nanotunnels and similar frequency in short distance nanotunnels with respect to D4C and WT-JPH2 myocytes (Online Table II and Figure 7M – between red arrows). To address whether these morphological modifications are associated with mitochondrial bioenergetics, we measured oxygen consumption rate (OCR) via a Seahorse analyzer (Figure 7R). No differences were found in basal respiration, ATP linked respiration and proton leak (Figure 7S, 7T and 7W, respectively). Notably, we found elevated maximal respiration and increased spare capacity in WT-JPH2 overexpressed myocytes (Figures 7U and 7V, respectively), suggesting that these myocytes could produce more ATP than D0 and D4C myocytes. mut[PG1]JPH2 did not have this mitochondrial capability to preserve bioenergetics achieved by WT JPH2 overexpression in myocytes. Nonetheless, mut[PG1]JPH2 myocytes could still sustain maximal respiration, and maintain normal mitochondrial spare capacity similarly to freshly isolated myocytes or D4C myocytes (Figure 7U–V).

DISCUSSION

JPH2 is a structural protein required for T-tubule maturation and cardiac dyad stabilization[19]. The LTCC has been shown to interact with JPH2 in skeletal muscle[42, 43]. The present study explored the idea that LTCCs interact with the Joining region in JPH2 in cardiomyocytes, and this interaction is crucial for the recruitment of LTCC to T-tubules, assembly of cardiac dyads and maintenance of normal myocyte Ca^{2+}.

Alteration of JPH2 abundance may promote LTCC membrane redistribution in LVH.

Studies in murine models and human hearts have linked reductions in JPH2 expression in the heart to cardiac pathology and heart failure[18, 70]. The present experiments showed that a large mammalian animal model with LVH induced by pressure overload had a reduced abundance of JPH2 in the cardiomyocyte PMs. Cardiac hypertrophy often precedes HF and establishes the earliest molecular processes leading to disturbed cardiomyocyte structural and functional remodeling[1, 70]. Our current results show that these early pathological changes *in vivo* include redistribution of JPH2 across the cardiomyocyte PM with modification of JPH2 localization and formation of aggregates. The nature of these aggregates remains unclear, yet we speculate that they could be linked to either JPH2 degradation or JPH2 turnover as cells remodel in response to pressure overload. In parallel, we also detected LTCC α1C and β2a redistribution across the PM as part of the cardiac hypertrophic remodeling. Interestingly, LVH caused reduction in the JPH2: LTCC α1C subunit expression ratio in the PM, suggesting that if JPH2 clusters with LTCC, the incidence of such clustering is downregulated in cardiac hypertrophy.

Our *in vitro* model utilized isolated AFVMs in primary culture, a model known to demonstrate time dependent reductions in T-tubule (and other) structures. Advantages of using a primary culture of AFVMs is the similarity in physiology of feline and human hearts (longer duration action potentials, βMHC dependent, slow contractions) and the survival of these myocytes in culture without Ca^{2+}overload[50, 51]. Similarly to observations in intact hypertrophic heart[1], the T-tubular network was found to be downregulated and disorganized in D4C compared to freshly isolated AFVMs. The mechanism responsible for T-tubule loss in *in vivo* hypertrophy and failure and *in vitro* cell culture models is not clear, and may or may not be related. Given that we observed similar changes in JPH2 staining patterns in LVH and in cultured AFVMs, we used this *in vitro* system to study the role of JPH2 and its Joining region in T-tubule remodeling. Our studies show T-tubule degradation in cultured AFVMs was associated with LTCC mobilization from T-tubules to the crest area of surface membranes. This idea was also supported by isopycnic ultracentrifugation studies that showed LTCC redistribution across the PM in cultured myocytes. Collectively, our results support a direct association between the Joining region of JPH2 and a1c subunit of the LTCC, which also suggests that altered expression of JPH2 could change the number and distribution of LTCCs in cardiomyocytes.

The role of the Joining region in JPH2.

The Joining region of JPH2 is located between two MORN motifs that are closely associated with the PM of T-tubules, making it a domain that could potentially interact with LTCC. Previously it was described that JPH2 interacted with the C-terminus of LTCC in skeletal muscle[43]. In another study, a region encompassing 216–399 amino acids in JPH2 was truncated, leading to disruption of JPH2-LTCC interaction in the triad[42]. The Joining region in JPH2 coincides to amino acids 143–284. We made a mut[PG1]JPH2 in which the length of JPH2 was preserved as were all its remaining domains. The mutated mut[PG1]JPH2 involved changes in several charged/polar amino acids that are presumably involved in protein-protein interaction with LTCC. We generated these mutations as an investigative tool to explore the structural importance of the Joining region in JPH2 and its functional role in EC coupling. Mutations in the Joining region have been previously identified in human subjects[18] and in murine studies[22], highlighting the relevance of our study to pathological abnormalities such as hypertrophic cardiomyopathy and arrhythmias that can lead to sudden death. Comparison of secondary and tertiary structures of mut[PG1]JPH2 versus WT-JPH2 validated that any structural changes introduced by the mutagenesis were explicitly taking place in the Joining region. Adenoviral infection of AFVMs with WT-JPH2 and mut[PG1]JPH2 in cultured myocytes resulted in distinct effects on JPH2 spatial localization, density and integrity (Figure 2A–F, K). While overexpressing WT-JPH2 restored JPH2 abundance across the cultured cardiomyocyte, overexpressing mut[PG1]JPH2 caused JPH2 to localize towards the sarcolemma, away from the T-tubule membranes. These changes were associated with the composition of T-tubule system, dyad frequency, and overall cardiomyocyte architecture. Our qualitative and quantitative characterization of T-tubule structure showed that restoring WT-JPH2 levels in cultured AFVMs restored T-tubules that were being degraded over time in culture. However, overexpressing mut[PG1]JPH2 exacerbated the remodeling of the gross T-tubule network. Our results show that WT-JPH2 overexpression in AFVMs caused an increase in dyad length in accordance with previously published work[20]. Nevertheless, the

frequency of dyads was profoundly reduced in mut^{PG1}JPH2 overexpressing myocytes (Figure 2L and Online Figure VI), without altering the total expression levels of Ca^{2+} handling proteins (Online Figure XI and Figure 7A–I). mut^{PG1}JPH2 construct contains normal MORN motifs on the N-terminus that should enable regular interaction with T-tubules. It also contains intact transmembrane domains on the C-terminus, which are responsible for docking JPH2 to the jSR membrane. These domains are essentially responsible for stabilizing the dyad by bringing closer the junctional complex between T-tubules and jSR. We conclude that the mutation of the Joining region solely was sufficient to cause the effects of cardiac dyads degradation and overall myofilament disorganization. Our results suggest that an association between JPH2 and LTCCs, which is lost in mut^{PG1}JPH2, is a major factor that determines JPH2-induced rescue of T-tubule structure in cultured AFVMs. This discovery supports the idea that the JPH2 Joining region is necessary for stabilization of T-tubules and assembly of cardiac dyads.

The Joining region in JPH2 interacts with LTCC.

We explored the hypothesis that LTCCs interact with the Joining region in JPH2. Co-IP and PLA studies indicated that mut^{PG1}JPH2 reduced the protein-protein interaction between LTCC α1C and JPH2 by ~30–40% (Figure 3A–F). Overexpressing mut^{PG1}JPH2 decreased the co-localization between JPH2 and LTCC, and between LTCC and RyR that would normally occur in the cardiac dyads. Given that dyads are more abundant in the T-tubules versus the sarcolemma (75% vs. 25%, respectively)[71, 72], our results strongly suggest that mut^{PG1}JPH2 reduced JPH2-LTCC interactions in the T-tubular dyads. PLA substantiated that the remaining JPH2-LTCC interactions appeared at the periphery of the cardiomyocyte. One possible explanation is that the Joining region in JPH2 recruits LTCC to the T-tubules, but in the absence of T-tubules, JPH2 and LTCCs eventually translocate to the sarcolemma. Sucrose density gradient separation of purified PM corroborated these data by showing that mut^{PG1}JPH2 overexpression in myocytes induced JPH2 and LTCC redistribution across the PM (Figure 3G). mut^{PG1}JPH2 overexpression induced ~40% reduction in JPH2-LTCC interaction. This is likely to alter EC coupling since the LTCC is an "amplifying switch" that initiates CICR. Previous studies showed that relocation of $I_{Ca,L}$ away from the t-tubules occurs in HF [39] and this is associated with altered Ca^{2+} regulation. Induction of an immature cardiac phenotype is commonly observed in pathological remodeling associated with HF. This usually includes reactivation of fetal gene expression and lack of T-tubules[39, 73]. The embryonic heart lacks T-tubules yet the heart manages to sustain contraction[2]. mut^{PG1}JPH2 appears to promote an immature cardiac phenotype similar to that seen in failing cardiomyocytes. Previously, it was established that JPH2 has a central role in the formation and stabilization of T-tubule[19, 74]. Our experiments showed that overexpression of WT JPH2 in AFVM in culture rescued the disruption of T-tubules while expression of mut^{PG1}JPH2 exacerbates this disruption. We also showed that when LTCC abundance was reduced via shRNA that silenced LTCC (α1C) expression, the ability of WT-JPH2 expression (Figure 4) to rescue T-tubules disruption was lost. These studies strongly suggest that a direct association between LTCC and the Joining region in JPH2 is necessary for LTCC recruitment to the T-tubules and that this association is critical for T-tubule stabilization and assembly of cardiac dyads.

Interaction between The Joining region in JPH2 and LTCC is important for efficient EC coupling.

Remodeling of T-tubules is a pivotal determinant of changes in Ca^{2+} transient properties in cardiomyocytes. Despite exhibiting structural abnormalities, mut^{PG1}JPH2 overexpressing myocytes had normal basal cytosolic Ca^{2+} transients. However, these cells developed abnormal pro-arrhythmic Ca^{2+} waves after exposure to β-adrenergic stimulation (Figure 5). This phenotype is similar to a clinical syndrome of catecholaminergic polymorphic ventricular tachycardia (CPVT), where patients have a normal phenotype at rest but develop arrhythmias in response to physical activity or emotional stress[75]. Human studies have identified two mutations in the JPH2 Joining region: E169K leading to atrial fibrillation[22] and S165F leading to hypertrophic cardiomyopathy[18]. These reports and our data support the idea that the Joining region – LTCC interaction is an important domain that when disrupted leads to aberrant Ca^{2+} regulation. The amplitude of average Ca^{2+} transient in mut^{PG1}JPH2 myocytes had smaller responses to Iso (Figure 5C), similarly to LVH isolated myocytes (Online Figure IC), indicating either a reduction of I_{Ca} trigger, or an inability to increase SR Ca^{2+} load with Iso stimulation[60]. The "shoulder" in WT JPH2 Ca^{2+} transient could occur from a variety of myocyte changes but in our studies was associated with action potential prolongation (Online Figure X D–G). Poorly organized dyads and loss of T-tubules in mut^{PG1}JPH2 myocytes, promote physical loss of Ca^{2+} release units (couplons)[9, 46]. This likely explains the reduced synchrony of Ca^{2+} release from couplons at baseline and after Iso stimulation in mut^{PG1}JPH2 myocytes. Our data also illustrated that mut^{PG1}JPH2 overexpressing myocytes demonstrated spontaneous Ca^{2+} releases and alternans, which are known precursors of lethal arrythmia[76]. Based on our observations (Figure 5H, K–L), we classified two types of alternans in mut^{PG1}JPH2 myocytes after Iso exposure. The first was delayed afterdepolarization-induced triggered activity (DAD), involving "leaky" RyR, which usually becomes deleterious during catecholamine stimulation[77]. DADs occurred in mut^{PG1}JPH2 myocytes as asynchronous Ca^{2+} release appearing right after normal Ca^{2+} wave. The underlying mechanism likely involves spontaneous Ca^{2+} release from an SR overloaded with Ca^{2+} as well as changes in RyR phosphorylation (pRyR 2814), likely due to activation of CaMKII (Figure 7A, C and E). The second type of alternans was early afterdepolarization (EAD), which is typically developed due to $I_{Ca,L}$ during the late plateau phase of action-potential[77]. EADs induced Ca^{2+} release at the edges of mut^{PG1}JPH2 cell without being able to propagate to the center of the cell. This commonly occurs in myocytes lacking T-tubules. We conclude that lack of T-tubules in mut^{PG1}JPH2 myocytes promotes Ca^{2+} alternans. The DADs and EAD seen in mut^{PG1}JPH2 myocytes indicate disruption of Ca^{2+} homeostasis. We distinguished between the effect mut^{PG1}JPH2 had during Iso stimulation on I_{Ca} trigger and SR Ca^{2+} release. Clearly, Iso caused a significant increase in $I_{Ca,L}$ (Figure 6A–B), suggesting that dispositioning LTCC away from the T-tubules did not alter their responsiveness to PKA-mediated phosphorylation. However, a positive shift in the voltage dependence of $I_{Ca,L}$ activation in mut^{PG1}JPH2 myocytes was detected at baseline and after Iso stimulation (Figure 6C–D), which may indicate abnormal voltage regulation in LTCC. Using super-resolution patch-clamp, we found compelling evidence that LTCCs in mut^{PG1}JPH2 myocytes translocate from T-tubules to the crest, where they remain functionality (Figure 6E–G). Changes in LTCC microdomain location were previously observed in HF[39] and in triggered ventricular arrythmia[37]. We show that this relocation can

be associated with disruption of LTCC-JPH2 interaction. Altogether, lack of T-tubules, reduced numbers of dyads and relocation of LTCC to the crest in mut[PG1]JPH2 myocytes negatively regulate LTCC coupling to RyR, likely resulting in "orphaned" RyRs[78] and reduced SR content (Figure 8). Indeed, SR Ca^{2+} release in mut[PG1]JPH2 myocytes was not elevated in response to Iso (Figure 6H–I), indicating defective Ca^{2+} regulation by the SR in these cells.

JPH2 Joining region contributes to intracellular Ca^{2+} stability and energy balance in cardiomyocyte.

Cardiac dyads are compartmentalized Ca^{2+} microsignaling domains where Ca^{2+} influx through LTCCs induce Ca^{2+} release from the jSR. In addition to activation of the contractile machinery, Ca^{2+} also regulates many processes in the cardiomyocyte, including bioenergetics and stress responses. Our data shows that mut[PG1]JPH2 overexpressing AFVMs had irregular Ca^{2+} regulation, affecting cellular Ca^{2+}-dependent regulation through activation of CaMKII – a major Ca^{2+} dependent regulator of cardiac function (Figure 7A, E). Overactivation of CaMKII has been linked to many cardiac pathologies including EADs and DADs arrhythmias, cardiomyopathy and HF[30, 37, 79]. We also found evidence for over activation of CaMKII (T287) (Figure 7A, C), which is known to phosphorylate downstream targets reportedly linked to "leaky" RyR and spontaneous SR Ca^{2+} release [30, 80]. Spontaneous SR Ca^{2+} releases were abolished in mut[PG1]JPH2 overexpressing myocytes once these cells were treated with KN93 – a known CaMKII inhibitor (Online Figure IXB). Collectively our results suggest that disruption of the JPH2/LTCC association by mutation of the Joining region leads to disturbed Ca^{2+} regulation.

Our study also identified a link between overexpression of WT-JPH2 and mut[PG1]JPH2 in AFVMs and cardiomyocyte bioenergetics. The link between mitochondrial function and beat-to-beat cytosolic Ca^{2+} is established by the mitochondrial capacity to buffer cytosolic Ca^{2+}, to sense energetic cellular demand, and to activate Ca^{2+} dependent mitochondrial enzymes participating in oxidative phosphorylation and ATP synthesis[24, 81]. We observed a high frequency of tight junctions between mitochondria in WT-JPH2 overexpressing myocytes, followed by increased spare capacity and increased maximal respiration (Figures 7L, U, V). This communication between adjacent mitochondria has been previously described to enable mitochondrial content exchange[67, 69]. Assuming that cell remodeling in culture is an energetically costly process, this type of mitochondrial communication may be bioenergetically protective because mitochondria in WT-JPH2 myocytes *in vitro* store excessive energy on demand. Parallel *in vivo* studies also showed that cardiac overexpression of JPH2 provided protective effects after pressure overload[20], although the mitochondrial function in these hearts was not explored. In mut[PG1]JPH2 overexpressing AFVMs, we found a different form of mitochondrial communication network – through long-distance nanotunnels. Similarly, it was found that RyR2A4860G[+/−] cardiomyocytes had increased incidence of long-distance nanotunnels, and surprisingly, the intermitochondrial matrix exchange rate via these nanotunnels was much slower[68]. It is considered that such mitochondrial communicating structures are 'reaching out for help'[69]. Indeed, we observed an exclusive stressful cellular environment in mut[PG1]JPH2 myocytes linked to the imbalance of Ca^{2+}, myofilament disorganization and loss of T-tubules. A

possible explanation is that mitochondria sense these abnormal cellular conditions, probably via changes in Ca^{2+}, and form contacts with distant mitochondria to maintain ATP production. This could also explain the increase in mitochondria size and shape change (Figure 7O–Q). Therefore, we postulate that the basal respiration, ATP-linked respiration, maximal respiration and spare capacity are preserved in mut[PG1]JPH2 myocytes, despite of remarkable reduction in mitochondria number (Figure 7N). We cannot entirely exclude mitochondrial fission/fusion processes, which are not the focus of this study.

In summary, this study demonstrates that LTCC α1C subunit interacts with the Joining region in JPH2 in cardiomyocyte PM. The studies performed showed that disruption of this interaction by mutagenesis in the Joining region led to significant structural alterations of the cardiac dyads and loss of T-tubules, followed by aberrant Ca^{2+} regulation and alterations of Ca^{2+}-dependent cellular processes (Figure 8). These finding suggest that the JPH2-LTCC interaction is critical to the normal function of cardiac myocytes.

Supplementary Material

Refer to Web version on PubMed Central for supplementary material.

Acknowledgments

Nonstandard Abbreviations and Acronyms:

T-tubules	Transverse tubules
EC coupling	Excitation contraction coupling
HF	Heart failure
PM	Plasma membrane
jSR	junctional sarcoplasmic reticulum
JPH2	Junctophilin 2
LTCC	L-type Ca^{2+} channel
RyR	Ryanodine receptor
CICR	Ca^{2+} induced Ca^{2+} release
AFVMs	Adult Feline ventricular myocytes
Ad	Adenovirus
LVH	Left ventricular hypertrophy

MORN	membrane occupation and recognition nexus
NCX	Sodium Calcium exchanger
ARVMs	Adult Rat ventricular myocytes
TEM	Transmission electron microscopy
SERCA2a	Sarcoplasmic reticulum calcium ATPase 2a
PLB	Phospholamban
CaMKII	Calcium/calmodulin-dependent kinase II
OCR	Oxygen consumption rate
CPVT	catecholaminergic polymorphic ventricular tachycardia
DAD	delayed afterdepolarization
EAD	early afterdepolarization

REFERENCES

1. Wei S, Guo A, Chen B, Kutschke W, Xie YP, Zimmerman K, Weiss RM, Anderson ME, Cheng H, Song LS. T-tubule remodeling during transition from hypertrophy to heart failure. Circulation research. 2010;107:520–531 [PubMed: 20576937]

2. Hong T, Shaw RM. Cardiac t-tubule microanatomy and function. Physiological reviews. 2017;97:227–252 [PubMed: 27881552]

3. Crossman DJ, Ruygrok PN, Soeller C, Cannell MB. Changes in the organization of excitation-contraction coupling structures in failing human heart. PloS one. 2011;6:e17901 [PubMed: 21408028]

4. Louch WE, Sejersted OM, Swift F. There goes the neighborhood: Pathological alterations in t-tubule morphology and consequences for cardiomyocyte ca2+ handling. Journal of biomedicine & biotechnology. 2010;2010:503906 [PubMed: 20396394]

5. Bito V, Heinzel FR, Weidemann F, Dommke C, van der Velden J, Verbeken E, Claus P, Bijnens B, De Scheerder I, Stienen GJ, Sutherland GR, Sipido KR. Cellular mechanisms of contractile dysfunction in hibernating myocardium. Circulation research. 2004;94:794–801 [PubMed: 15001528]

6. Pinali C, Malik N, Davenport JB, Allan LJ, Murfitt L, Iqbal MM, Boyett MR, Wright EJ, Walker R, Zhang Y, Dobryznski H, Holt CM, Kitmitto A. Post-myocardial infarction t-tubules form enlarged branched structures with dysregulation of junctophilin-2 and bridging integrator 1 (bin-1). Journal of the American Heart Association. 2017;6

7. Brette F, Orchard C. T-tubule function in mammalian cardiac myocytes. Circulation research. 2003;92:1182–1192 [PubMed: 12805236]

8. Lyon AR, MacLeod KT, Zhang Y, Garcia E, Kanda GK, Lab MJ, Korchev YE, Harding SE, Gorelik J. Loss of t-tubules and other changes to surface topography in ventricular myocytes from failing human and rat heart. Proceedings of the National Academy of Sciences of the United States of America. 2009;106:6854–6859 [PubMed: 19342485]

9. Heinzel FR, Bito V, Biesmans L, Wu M, Detre E, von Wegner F, Claus P, Dymarkowski S, Maes F, Bogaert J, Rademakers F, D'Hooge J, Sipido K. Remodeling of t-tubules and reduced synchrony of ca2+ release in myocytes from chronically ischemic myocardium. Circulation research. 2008;102:338–346 [PubMed: 18079411]

10. He J, Conklin MW, Foell JD, Wolff MR, Haworth RA, Coronado R, Kamp TJ. Reduction in density of transverse tubules and l-type ca(2+) channels in canine tachycardia-induced heart failure. Cardiovascular research. 2001;49:298–307 [PubMed: 11164840]

11. Ibrahim M, Gorelik J, Yacoub MH, Terracciano CM. The structure and function of cardiac t-tubules in health and disease. Proceedings. Biological sciences. 2011;278:2714–2723 [PubMed: 21697171]

12. Garbino A, Wehrens XH. Emerging role of junctophilin-2 as a regulator of calcium handling in the heart. Acta pharmacologica Sinica. 2010;31:1019–1021 [PubMed: 20694023]

13. Nishi M, Mizushima A, Nakagawara K, Takeshima H. Characterization of human junctophilin subtype genes. Biochemical and biophysical research communications. 2000;273:920–927 [PubMed: 10891348]

14. Chen B, Guo A, Zhang C, Chen R, Zhu Y, Hong J, Kutschke W, Zimmerman K, Weiss RM, Zingman L, Anderson ME, Wehrens XH, Song LS. Critical roles of junctophilin-2 in t-tubule and excitation-contraction coupling maturation during postnatal development. Cardiovascular research. 2013;100:54–62 [PubMed: 23860812]

15. Orchard C, Brette F. T-tubules and sarcoplasmic reticulum function in cardiac ventricular myocytes. Cardiovascular research. 2008;77:237–244 [PubMed: 18006490]

16. van Oort RJ, Garbino A, Wang W, Dixit SS, Landstrom AP, Gaur N, De Almeida AC, Skapura DG, Rudy Y, Burns AR, Ackerman MJ, Wehrens XH. Disrupted junctional membrane complexes and hyperactive ryanodine receptors after acute junctophilin knockdown in mice. Circulation. 2011;123:979–988 [PubMed: 21339484]

17. Landstrom AP, Kellen CA, Dixit SS, van Oort RJ, Garbino A, Weisleder N, Ma J, Wehrens XH, Ackerman MJ. Junctophilin-2 expression silencing causes cardiocyte hypertrophy and abnormal intracellular calcium-handling. Circulation. Heart failure. 2011;4:214–223 [PubMed: 21216834]

18. Landstrom AP, Weisleder N, Batalden KB, Bos JM, Tester DJ, Ommen SR, Wehrens XH, Claycomb WC, Ko JK, Hwang M, Pan Z, Ma J, Ackerman MJ. Mutations in jph2-encoded junctophilin-2 associated with hypertrophic cardiomyopathy in humans. Journal of molecular and cellular cardiology. 2007;42:1026–1035 [PubMed: 17509612]

19. Reynolds JO, Chiang DY, Wang W, Beavers DL, Dixit SS, Skapura DG, Landstrom AP, Song LS, Ackerman MJ, Wehrens XH. Junctophilin-2 is necessary for t-tubule maturation during mouse heart development. Cardiovascular research. 2013;100:44–53 [PubMed: 23715556]

20. Guo A, Zhang X, Iyer VR, Chen B, Zhang C, Kutschke WJ, Weiss RM, Franzini-Armstrong C, Song LS. Overexpression of junctophilin-2 does not enhance baseline function but attenuates heart failure development after cardiac stress. Proceedings of the National Academy of Sciences of the United States of America. 2014;111:12240–12245 [PubMed: 25092313]

21. Zhang C, Chen B, Guo A, Zhu Y, Miller JD, Gao S, Yuan C, Kutschke W, Zimmerman K, Weiss RM, Wehrens XH, Hong J, Johnson FL, Santana LF, Anderson ME, Song LS. Microtubule-mediated defects in junctophilin-2 trafficking contribute to myocyte transverse-tubule remodeling and ca2+ handling dysfunction in heart failure. Circulation. 2014;129:1742–1750 [PubMed: 24519927]

22. Beavers DL, Wang W, Ather S, Voigt N, Garbino A, Dixit SS, Landstrom AP, Li N, Wang Q, Olivotto I, Dobrev D, Ackerman MJ, Wehrens XHT. Mutation e169k in junctophilin-2 causes atrial fibrillation due to impaired ryr2 stabilization. Journal of the American College of Cardiology. 2013;62:2010–2019 [PubMed: 23973696]

23. Minamisawa S, Oshikawa J, Takeshima H, Hoshijima M, Wang Y, Chien KR, Ishikawa Y, Matsuoka R. Junctophilin type 2 is associated with caveolin-3 and is down-regulated in the hypertrophic and dilated cardiomyopathies. Biochemical and biophysical research communications. 2004;325:852–856 [PubMed: 15541368]

24. Bers DM. Calcium cycling and signaling in cardiac myocytes. Annual review of physiology. 2008;70:23–49

25. Bers DM. Cardiac excitation-contraction coupling. Nature. 2002;415:198–205 [PubMed: 11805843]

26. Scriven DR, Dan P, Moore ED. Distribution of proteins implicated in excitation-contraction coupling in rat ventricular myocytes. Biophysical journal. 2000;79:2682–2691 [PubMed: 11053140]

27. Gomez AM, Valdivia HH, Cheng H, Lederer MR, Santana LF, Cannell MB, McCune SA, Altschuld RA, Lederer WJ. Defective excitation-contraction coupling in experimental cardiac hypertrophy and heart failure. Science. 1997;276:800–806 [PubMed: 9115206]

28. Hobai IA, O'Rourke B. Decreased sarcoplasmic reticulum calcium content is responsible for defective excitation-contraction coupling in canine heart failure. Circulation. 2001;103:1577–1584 [PubMed: 11257088]

29. Beuckelmann DJ. Contributions of ca(2+)-influx via the l-type ca(2+)-current and ca(2+)-release from the sarcoplasmic reticulum to [ca2+]i-transients in human myocytes. Basic research in cardiology. 1997;92 Suppl 1:105–110 [PubMed: 9202850]

30. Bers DM, Grandi E. Calcium/calmodulin-dependent kinase ii regulation of cardiac ion channels. Journal of cardiovascular pharmacology. 2009;54:180–187 [PubMed: 19333131]

31. Rosca MG, Tandler B, Hoppel CL. Mitochondria in cardiac hypertrophy and heart failure. Journal of molecular and cellular cardiology. 2013;55:31–41 [PubMed: 22982369]

32. Mukherjee R, Spinale FG. L-type calcium channel abundance and function with cardiac hypertrophy and failure: A review. Journal of molecular and cellular cardiology. 1998;30:1899–1916 [PubMed: 9799645]

33. Houser SR. Reduced abundance of transverse tubules and l-type calcium channels: Another cause of defective contractility in failing ventricular myocytes. Cardiovascular research. 2001;49:253–256 [PubMed: 11164835]

34. Chen X, Piacentino V 3rd, Furukawa S, Goldman B, Margulies KB, Houser SR. L-type ca2+ channel density and regulation are altered in failing human ventricular myocytes and recover after support with mechanical assist devices. Circulation research. 2002;91:517–524 [PubMed: 12242270]

35. Chien AJ, Zhao X, Shirokov RE, Puri TS, Chang CF, Sun D, Rios E, Hosey MM. Roles of a membrane-localized beta subunit in the formation and targeting of functional l-type ca2+ channels. The Journal of biological chemistry. 1995;270:30036–30044 [PubMed: 8530407]

36. Catalucci D, Zhang DH, DeSantiago J, Aimond F, Barbara G, Chemin J, Bonci D, Picht E, Rusconi F, Dalton ND, Peterson KL, Richard S, Bers DM, Brown JH, Condorelli G. Akt regulates l-type ca2+ channel activity by modulating cavalpha1 protein stability. The Journal of cell biology. 2009;184:923–933 [PubMed: 19307602]

37. Sanchez-Alonso JL, Bhargava A, O'Hara T, Glukhov AV, Schobesberger S, Bhogal N, Sikkel MB, Mansfield C, Korchev YE, Lyon AR, Punjabi PP, Nikolaev VO, Trayanova NA, Gorelik J. Microdomain-specific modulation of l-type calcium channels leads to triggered ventricular arrhythmia in heart failure. Circulation research. 2016;119:944–955 [PubMed: 27572487]

38. Hong TT, Smyth JW, Chu KY, Vogan JM, Fong TS, Jensen BC, Fang K, Halushka MK, Russell SD, Colecraft H, Hoopes CW, Ocorr K, Chi NC, Shaw RM. Bin1 is reduced and cav1.2 trafficking is impaired in human failing cardiomyocytes. Heart rhythm. 2012;9:812–820 [PubMed: 22138472]

39. Bryant SM, Kong CH, Watson J, Cannell MB, James AF, Orchard CH. Altered distribution of ica impairs ca release at the t-tubules of ventricular myocytes from failing hearts. Journal of molecular and cellular cardiology. 2015;86:23–31 [PubMed: 26103619]

40. Yamaguchi H, Hara M, Strobeck M, Fukasawa K, Schwartz A, Varadi G. Multiple modulation pathways of calcium channel activity by a beta subunit. Direct evidence of beta subunit participation in membrane trafficking of the alpha1c subunit. The Journal of biological chemistry. 1998;273:19348–19356 [PubMed: 9668125]

41. Hong TT, Smyth JW, Gao D, Chu KY, Vogan JM, Fong TS, Jensen BC, Colecraft HM, Shaw RM. Bin1 localizes the l-type calcium channel to cardiac t-tubules. PLoS biology. 2010;8:e1000312 [PubMed: 20169111]

42. Golini L, Chouabe C, Berthier C, Cusimano V, Fornaro M, Bonvallet R, Formoso L, Giacomello E, Jacquemond V, Sorrentino V. Junctophilin 1 and 2 proteins interact with the l-type ca2+ channel dihydropyridine receptors (dhprs) in skeletal muscle. The Journal of biological chemistry. 2011;286:43717–43725 [PubMed: 22020936]

43. Nakada T, Kashihara T, Komatsu M, Kojima K, Takeshita T, Yamada M. Physical interaction of junctophilin and the cav1.1 c terminus is crucial for skeletal muscle contraction. Proceedings of the National Academy of Sciences of the United States of America. 2018;115:4507–4512 [PubMed: 29632175]

44. Poulet C, Sanchez-Alonso J, Swiatlowska P, Mouy F, Lucarelli C, Alvarez-Laviada A, Gross P, Terracciano C, Houser S, Gorelik J. Junctophilin-2 tethers t-tubules and recruits functional l-type calcium channels to lipid rafts in adult cardiomyocytes. Cardiovascular research. 2020

45. Wallner M, Eaton DM, Berretta RM, Borghetti G, Wu J, Baker ST, Feldsott EA, Sharp TE 3rd, Mohsin S, Oyama MA, von Lewinski D, Post H, Wolfson MR, Houser SR. A feline hfpef model with pulmonary hypertension and compromised pulmonary function. Scientific reports. 2017;7:16587 [PubMed: 29185443]

46. Harris DM, Mills GD, Chen X, Kubo H, Berretta RM, Votaw VS, Santana LF, Houser SR. Alterations in early action potential repolarization causes localized failure of sarcoplasmic reticulum ca2+ release. Circulation research. 2005;96:543–550 [PubMed: 15705962]

47. Mitcheson JS, Hancox JC, Levi AJ. Action potentials, ion channel currents and transverse tubule density in adult rabbit ventricular myocytes maintained for 6 days in cell culture. Pflugers Archiv : European journal of physiology. 1996;431:814–827 [PubMed: 8927497]

48. Lipp P, Huser J, Pott L, Niggli E. Spatially non-uniform ca2+ signals induced by the reduction of transverse tubules in citrate-loaded guinea-pig ventricular myocytes in culture. The Journal of physiology. 1996;497 (Pt 3):589–597 [PubMed: 9003546]

49. Bailey BA, Houser SR. Calcium transients in feline left ventricular myocytes with hypertrophy induced by slow progressive pressure overload. Journal of molecular and cellular cardiology. 1992;24:365–373 [PubMed: 1535666]

50. Pollack PS, Carson NL, Nuss HB, Marino TA, Houser SR. Mechanical properties of adult feline ventricular myocytes in culture. The American journal of physiology. 1991;260:H234–241 [PubMed: 1992803]

51. Peter AK, Bjerke MA, Leinwand LA. Biology of the cardiac myocyte in heart disease. Molecular biology of the cell. 2016;27:2149–2160 [PubMed: 27418636]

52. Shaw RM, Colecraft HM. L-type calcium channel targeting and local signalling in cardiac myocytes. Cardiovascular research. 2013;98:177–186 [PubMed: 23417040]

53. Louch WE, Bito V, Heinzel FR, Macianskiene R, Vanhaecke J, Flameng W, Mubagwa K, Sipido KR. Reduced synchrony of ca2+ release with loss of t-tubules-a comparison to ca2+ release in human failing cardiomyocytes. Cardiovascular research. 2004;62:63–73 [PubMed: 15023553]

54. Bers DM. Cardiac na/ca exchange function in rabbit, mouse and man: What's the difference? Journal of molecular and cellular cardiology. 2002;34:369–373 [PubMed: 11991726]

55. Duthinh V, Houser SR. Contractile properties of single isolated feline ventriculocytes. The American journal of physiology. 1988;254:H59–66 [PubMed: 3337260]

56. Silver LH, Hemwall EL, Marino TA, Houser SR. Isolation and morphology of calcium-tolerant feline ventricular myocytes. The American journal of physiology. 1983;245:H891–896 [PubMed: 6638207]

57. Wickenden AD, Kaprielian R, Kassiri Z, Tsoporis JN, Tsushima R, Fishman GI, Backx PH. The role of action potential prolongation and altered intracellular calcium handling in the pathogenesis of heart failure. Cardiovascular research. 1998;37:312–323 [PubMed: 9614488]

58. Kallberg M, Wang H, Wang S, Peng J, Wang Z, Lu H, Xu J. Template-based protein structure modeling using the raptorx web server. Nature protocols. 2012;7:1511–1522 [PubMed: 22814390]

59. Peng J, Xu J. Raptorx: Exploiting structure information for protein alignment by statistical inference. Proteins. 2011;79 Suppl 10:161–171 [PubMed: 21987485]

60. Ginsburg KS, Bers DM. Modulation of excitation-contraction coupling by isoproterenol in cardiomyocytes with controlled sr ca2+ load and ca2+ current trigger. The Journal of physiology. 2004;556:463–480 [PubMed: 14724205]

61. Song LS, Wang SQ, Xiao RP, Spurgeon H, Lakatta EG, Cheng H. Beta-adrenergic stimulation synchronizes intracellular ca(2+) release during excitation-contraction coupling in cardiac myocytes. Circulation research. 2001;88:794–801 [PubMed: 11325871]

62. Bhargava A, Lin X, Novak P, Mehta K, Korchev Y, Delmar M, Gorelik J. Super-resolution scanning patch clamp reveals clustering of functional ion channels in adult ventricular myocyte. Circulation research. 2013;112:1112–1120 [PubMed: 23438901]

63. Fu Y, Hong T. Bin1 regulates dynamic t-tubule membrane. Biochimica et biophysica acta. 2016;1863:1839–1847 [PubMed: 26578114]

64. Ishida A, Kitani T, Fujisawa H. Evidence that autophosphorylation at thr-286/thr-287 is required for full activation of calmodulin-dependent protein kinase ii. Biochimica et biophysica acta. 1996;1311:211–217 [PubMed: 8664349]

65. Respress JL, van Oort RJ, Li N, Rolim N, Dixit SS, deAlmeida A, Voigt N, Lawrence WS, Skapura DG, Skardal K, Wisloff U, Wieland T, Ai X, Pogwizd SM, Dobrev D, Wehrens XH. Role of ryr2 phosphorylation at s2814 during heart failure progression. Circulation research. 2012;110:1474–1483 [PubMed: 22511749]

66. Mills GD, Kubo H, Harris DM, Berretta RM, Piacentino V, 3rd, Houser SR. Phosphorylation of phospholamban at threonine-17 reduces cardiac adrenergic contractile responsiveness in chronic pressure overload-induced hypertrophy. American journal of physiology. Heart and circulatory physiology. 2006;291:H61–70 [PubMed: 16772527]

67. Huang X, Sun L, Ji S, Zhao T, Zhang W, Xu J, Zhang J, Wang Y, Wang X, Franzini-Armstrong C, Zheng M, Cheng H. Kissing and nanotunneling mediate intermitochondrial communication in the heart. Proceedings of the National Academy of Sciences of the United States of America. 2013;110:2846–2851 [PubMed: 23386722]

68. Lavorato M, Iyer VR, Dewight W, Cupo RR, Debattisti V, Gomez L, De la Fuente S, Zhao YT, Valdivia HH, Hajnoczky G, Franzini-Armstrong C. Increased mitochondrial nanotunneling activity, induced by calcium imbalance, affects intermitochondrial matrix exchanges. Proceedings of the National Academy of Sciences of the United States of America. 2017;114:E849–E858 [PubMed: 28096415]

69. Vincent AE, Turnbull DM, Eisner V, Hajnoczky G, Picard M. Mitochondrial nanotunnels. Trends in cell biology. 2017;27:787–799 [PubMed: 28935166]

70. Landstrom AP, Beavers DL, Wehrens XH. The junctophilin family of proteins: From bench to bedside. Trends in molecular medicine. 2014;20:353–362 [PubMed: 24636942]

71. Brette F, Orchard C. Resurgence of cardiac t-tubule research. Physiology. 2007;22:167–173 [PubMed: 17557937]

72. Brette F, Salle L, Orchard CH. Quantification of calcium entry at the t-tubules and surface membrane in rat ventricular myocytes. Biophysical journal. 2006;90:381–389 [PubMed: 16214862]

73. Lipsett DB, Frisk M, Aronsen JM, Norden ES, Buonarati OR, Cataliotti A, Hell JW, Sjaastad I, Christensen G, Louch WE. Cardiomyocyte substructure reverts to an immature phenotype during heart failure. The Journal of physiology. 2019;597:1833–1853 [PubMed: 30707448]

74. Liang X, Mei Y, Huang X, Shen G, Zhu D, Yu Y, Wang J, Lou Y. Junctophilin 2 knockdown interfere with mitochondrium status in esc-cms and cardiogenesis of es cells. Journal of cellular biochemistry. 2012;113:2884–2894 [PubMed: 22511307]

75. Zhao YT, Valdivia CR, Gurrola GB, Powers PP, Willis BC, Moss RL, Jalife J, Valdivia HH. Arrhythmogenesis in a catecholaminergic polymorphic ventricular tachycardia mutation that depresses ryanodine receptor function. Proceedings of the National Academy of Sciences of the United States of America. 2015;112:E1669–1677 [PubMed: 25775566]

76. Rosenbaum DS. T wave alternans: A mechanism of arrhythmogenesis comes of age after 100 years. Journal of cardiovascular electrophysiology. 2001;12:207–209 [PubMed: 11232620]

77. Antzelevitch C, Burashnikov A. Overview of basic mechanisms of cardiac arrhythmia. Cardiac electrophysiology clinics. 2011;3:23–45 [PubMed: 21892379]

78. Song LS, Sobie EA, McCulle S, Lederer WJ, Balke CW, Cheng H. Orphaned ryanodine receptors in the failing heart. Proceedings of the National Academy of Sciences of the United States of America. 2006;103:4305–4310 [PubMed: 16537526]

79. Hudmon A, Schulman H, Kim J, Maltez JM, Tsien RW, Pitt GS. Camkii tethers to l-type ca2+ channels, establishing a local and dedicated integrator of ca2+ signals for facilitation. The Journal of cell biology. 2005;171:537–547 [PubMed: 16275756]

80. Makarewich CA, Zhang H, Davis J, Correll RN, Trappanese DM, Hoffman NE, Troupes CD, Berretta RM, Kubo H, Madesh M, Chen X, Gao E, Molkentin JD, Houser SR. Transient receptor potential channels contribute to pathological structural and functional remodeling after myocardial infarction. Circulation research. 2014;115:567–580 [PubMed: 25047165]

81. Dedkova EN, Blatter LA. Calcium signaling in cardiac mitochondria. Journal of molecular and cellular cardiology. 2013;58:125–133 [PubMed: 23306007]

82. Chen X, Wilson RM, Kubo H, Berretta RM, Harris DM, Zhang X, Jaleel N, MacDonnell SM, Bearzi C, Tillmanns J, Trofimova I, Hosoda T, Mosna F, Cribbs L, Leri A, Kajstura J, Anversa P, Houser SR. Adolescent feline heart contains a population of small, proliferative ventricular myocytes with immature physiological properties. Circulation research. 2007;100:536–544 [PubMed: 17272809]

83. Guo A, Song LS. Autott: Automated detection and analysis of t-tubule architecture in cardiomyocytes. Biophysical journal. 2014;106:2729–2736 [PubMed: 24940790]

84. Duran JM, Taghavi S, Berretta RM, Makarewich CA, Sharp Iii T, Starosta T, Udeshi F, George JC, Kubo H, Houser SR. A characterization and targeting of the infarct border zone in a swine model of myocardial infarction. Clinical and translational science. 2012;5:416–421 [PubMed: 23067355]

85. Kubo H, Margulies KB, Piacentino V 3rd, Gaughan JP, Houser SR. Patients with end-stage congestive heart failure treated with beta-adrenergic receptor antagonists have improved ventricular myocyte calcium regulatory protein abundance. Circulation. 2001;104:1012–1018 [PubMed: 11524394]

86. Carlile-Klusacek M, Rizzo V. Endothelial cytoskeletal reorganization in response to par1 stimulation is mediated by membrane rafts but not caveolae. American journal of physiology. Heart and circulatory physiology. 2007;293:H366–375 [PubMed: 17369462]

87. Trappanese DM, Liu Y, McCormick RC, Cannavo A, Nanayakkara G, Baskharoun MM, Jarrett H, Woitek FJ, Tillson DM, Dillon AR, Recchia FA, Balligand JL, Houser SR, Koch WJ, Dell'Italia LJ, Tsai EJ. Chronic beta1-adrenergic blockade enhances myocardial beta3-adrenergic coupling with nitric oxide-cgmp signaling in a canine model of chronic volume overload: New insight into mechanisms of cardiac benefit with selective beta1-blocker therapy. Basic research in cardiology. 2015;110:456 [PubMed: 25480109]

88. Lavorato M, Huang TQ, Iyer VR, Perni S, Meissner G, Franzini-Armstrong C. Dyad content is reduced in cardiac myocytes of mice with impaired calmodulin regulation of ryr2. Journal of muscle research and cell motility. 2015;36:205–214 [PubMed: 25694159]

89. Jayasinghe ID, Baddeley D, Kong CH, Wehrens XH, Cannell MB, Soeller C. Nanoscale organization of junctophilin-2 and ryanodine receptors within peripheral couplings of rat ventricular cardiomyocytes. Biophysical journal. 2012;102:L19–21 [PubMed: 22404946]

90. Jayasinghe ID, Munro M, Baddeley D, Launikonis BS, Soeller C. Observation of the molecular organization of calcium release sites in fast- and slow-twitch skeletal muscle with nanoscale imaging. Journal of the Royal Society, Interface. 2014;11

91. Otsu N A threshold selection method from gray-level histograms. IEEE Transactions on Systems, Man, and Cybernetics. 1979;9:62–66

92. Zhang H, Chen X, Gao E, MacDonnell SM, Wang W, Kolpakov M, Nakayama H, Zhang X, Jaleel N, Harris DM, Li Y, Tang M, Berretta R, Leri A, Kajstura J, Sabri A, Koch WJ, Molkentin JD, Houser SR. Increasing cardiac contractility after myocardial infarction exacerbates cardiac injury and pump dysfunction. Circulation research. 2010;107:800–809 [PubMed: 20671241]

93. Zhang H, Makarewich CA, Kubo H, Wang W, Duran JM, Li Y, Berretta RM, Koch WJ, Chen X, Gao E, Valdivia HH, Houser SR. Hyperphosphorylation of the cardiac ryanodine receptor at serine 2808 is not involved in cardiac dysfunction after myocardial infarction. Circulation research. 2012;110:831–840 [PubMed: 22302785]

94. Chen X, Zhang X, Harris DM, Piacentino V, 3rd, Berretta RM, Margulies KB, Houser SR. Reduced effects of bay k 8644 on l-type ca2+ current in failing human cardiac myocytes are related to abnormal adrenergic regulation. American journal of physiology. Heart and circulatory physiology. 2008;294:H2257–2267 [PubMed: 18359894]

95. Novak P, Gorelik J, Vivekananda U, Shevchuk AI, Ermolyuk YS, Bailey RJ, Bushby AJ, Moss GW, Rusakov DA, Klenerman D, Kullmann DM, Volynski KE, Korchev YE. Nanoscale-targeted

patch-clamp recordings of functional presynaptic ion channels. Neuron. 2013;79:1067–1077 [PubMed: 24050398]

96. Ye P, Sheng L, Zhang C, Liu Y. Atorvastatin attenuating down-regulation of peroxisome proliferator-activated receptor gamma in preventing cardiac hypertrophy of rats in vitro and in vivo. Journal of pharmacy & pharmaceutical sciences : a publication of the Canadian Society for Pharmaceutical Sciences, Societe canadienne des sciences pharmaceutiques. 2006;9:365–375

97. Barbe MF, Krueger JJ, Loomis R, Otte J, Gordon J. Memory deficits, gait ataxia and neuronal loss in the hippocampus and cerebellum in mice that are heterozygous for pur-alpha. Neuroscience. 2016;337:177–190 [PubMed: 27651147]

NOVELTY AND SIGNIFICANCE

What Is Known?

- Diseased hearts including failing hearts have disrupted junctional membrane complexes.

- Junctophilin-2 (JPH2) is a crucial component of junctional membrane complexes in cardiac cells, that facilitates crosstalk between cell surface and intracellular ion channels.

- The Joining region in JPH2 is a conservative structural domain but its role in JPH2 function has not been determined.

What New Information Does This Article Contribute?

- The Joining region in JPH2 interacts with cell surface ion channels, known as L-type Ca^{2+} channels (LTCCs), and mediates their recruitment into the junctional membrane complexes in cardiac cells.

- Alteration of JPH2 abundance in cardiac hypertrophy promotes LTCC membrane redistribution away from the junctional complexes.

- The Joining region in JPH2 contributes to the stabilization of junctional membrane structures, intracellular Ca^{2+} stability and bioenergetic balance.

JPH2 is a critical regulator of cardiomyocyte membrane junctions by tethering sarcoplasmic reticulum and transverse-tubule (T-tubule) membranes. Thereby, JPH2 brings their residing ion channels into a close proximity to ensure normal Ca^{2+} cycling. We asked how JPH2 holds LTCCs in T-tubules to maintain their function with every heartbeat. We found that the Joining region in JPH2 is a novel interaction site between JPH2 and LTCC, and this interaction is crucial for LTCC recruitment to the T-tubules. In cardiac disease, reduced JPH2 membrane abundance promoted LTCC membrane displacement away from T-tubules. Our studies showed that alteration of the Joining region resulted in structural abnormalities of T-tubules and redistribution of LTCCs to other membrane locations. Cardiac cells with disrupted Joining region in JPH2 developed pro-arrhythmic Ca^{2+} waves after adrenergic stimulation, indicating that the interaction between the Joining region in JPH2 and LTCC is important for intracellular Ca^{2+} stability. Disruption of this interaction site caused irregular Ca^{2+} signaling through activation of Ca^{2+}/calmodulin-dependent protein kinase II – a major Ca^{2+} dependent regulator of cardiac function. These changes also impacted cellular bioenergetics regulation. In summary, this study demonstrates that LTCC interaction with the Joining region in JPH2 is critical to the normal function of cardiomyocytes.
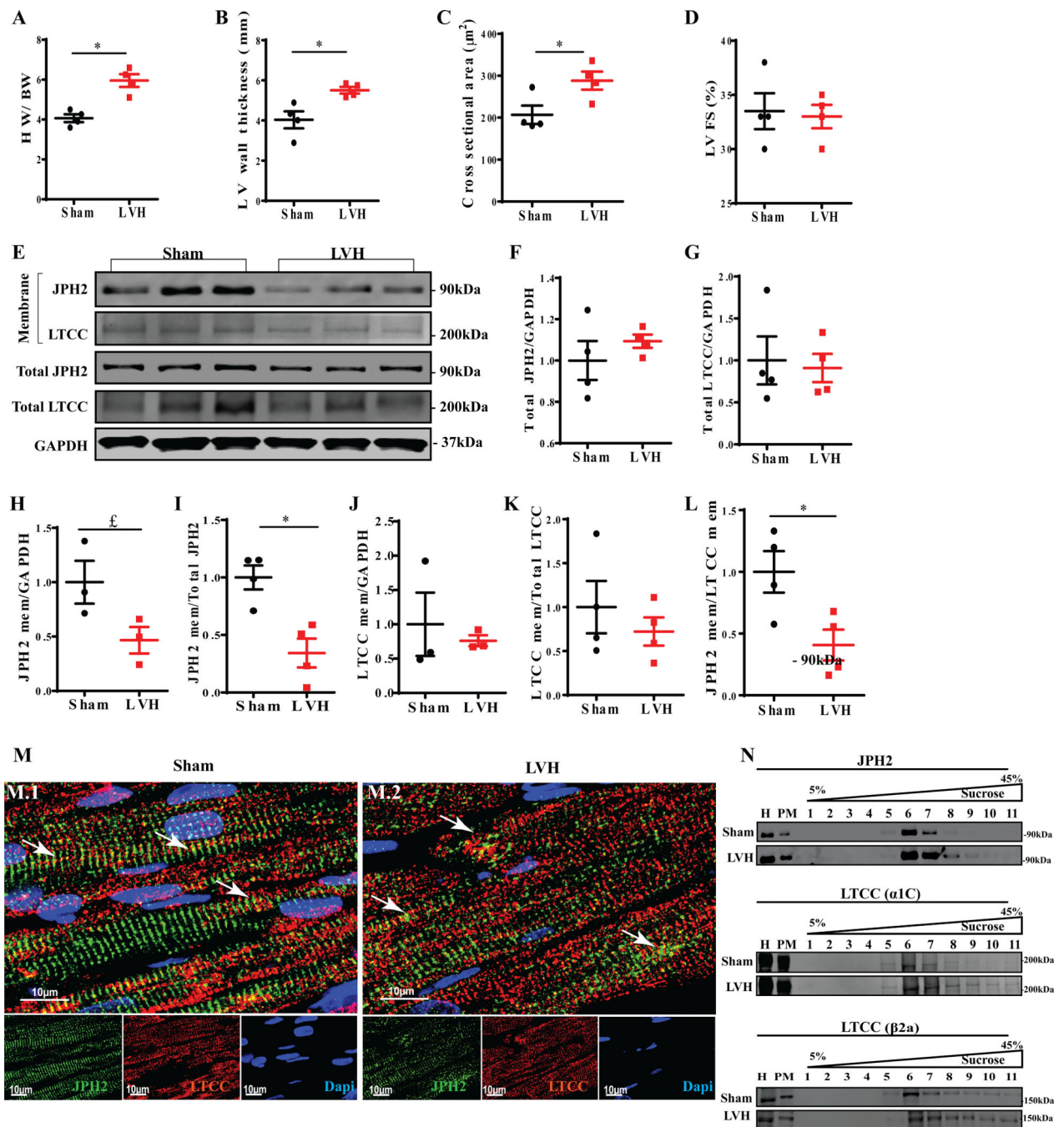
Figure 1. LVH in Feline hearts induces reductions of JPH2 abundance in the PM and shifts the membrane localization of JPH2 and LTCC.

The LV hypertrophic phenotype in banded Felines was determined by the following parameters: **(A)** increased heart weight to body weight ratio (HW/BW); **(B)** enlarged LV wall thickness. **For A and B:** Data are shown as mean ± SEM, N=4 Felines, *P=0.0286 LVH vs. sham using non-parametric Mann Whitney test; **(C)** Increased cardiomyocyte cross sectional area. Data are shown as means ± SEM, N=4 Felines, n=10 images per Feline, *P=0.0381 LVH vs. sham using unpaired t-test; and **(D)** preserved LV fractional shortening

(FS). Data are shown as mean ± SEM, N=4 Felines. A non-parametric Mann Whitney test was applied. **(E)** Representative immunoblotting of PM fractions extracted from Feline heart tissues and whole tissue lysates. **(F)** Comparison between LVH and sham densitometry analysis of total JPH2 expression and **(G)** total LTCC expression (non-parametric Mann Whitney was applied). **(H)** Summary of densitometry analysis of JPH2 membranal fraction abundance normalized to GAPDH (£P=0.098 LVH vs. sham using non-parametric Mann Whitney test) and **(I)** normalized to total JPH2 (*P=0.0286 LVH vs. sham using non-parametric Mann Whitney test). **(J)** Summary of densitometry analysis of LTCC membranal fraction abundance normalized to GAPDH and **(K)** normalized to total LTCC (non-parametric Mann Whitney test was applied). **(L)** Expression ratio of JPH2 membranal fraction normalized to LTCC (α1C) membranal fraction. (*P=0.05 LVH vs. sham using non-parametric Mann Whitney test). N=4 hearts per group. **(M)** Representative immunofluorescence images of JPH2 and LTCC (α1C) staining in sham **(M.1)** and LVH **(M.2)** Feline hearts. Arrows indicate the difference in JPH2 organization and colocalization with LTCC. Scale 10μm. **(N)** Representative Western blots of JPH2, LTCC (α1C) and LTCC (β2a) across sucrose density gradient fractions (F1–F11) of sham and LVH Feline hearts.
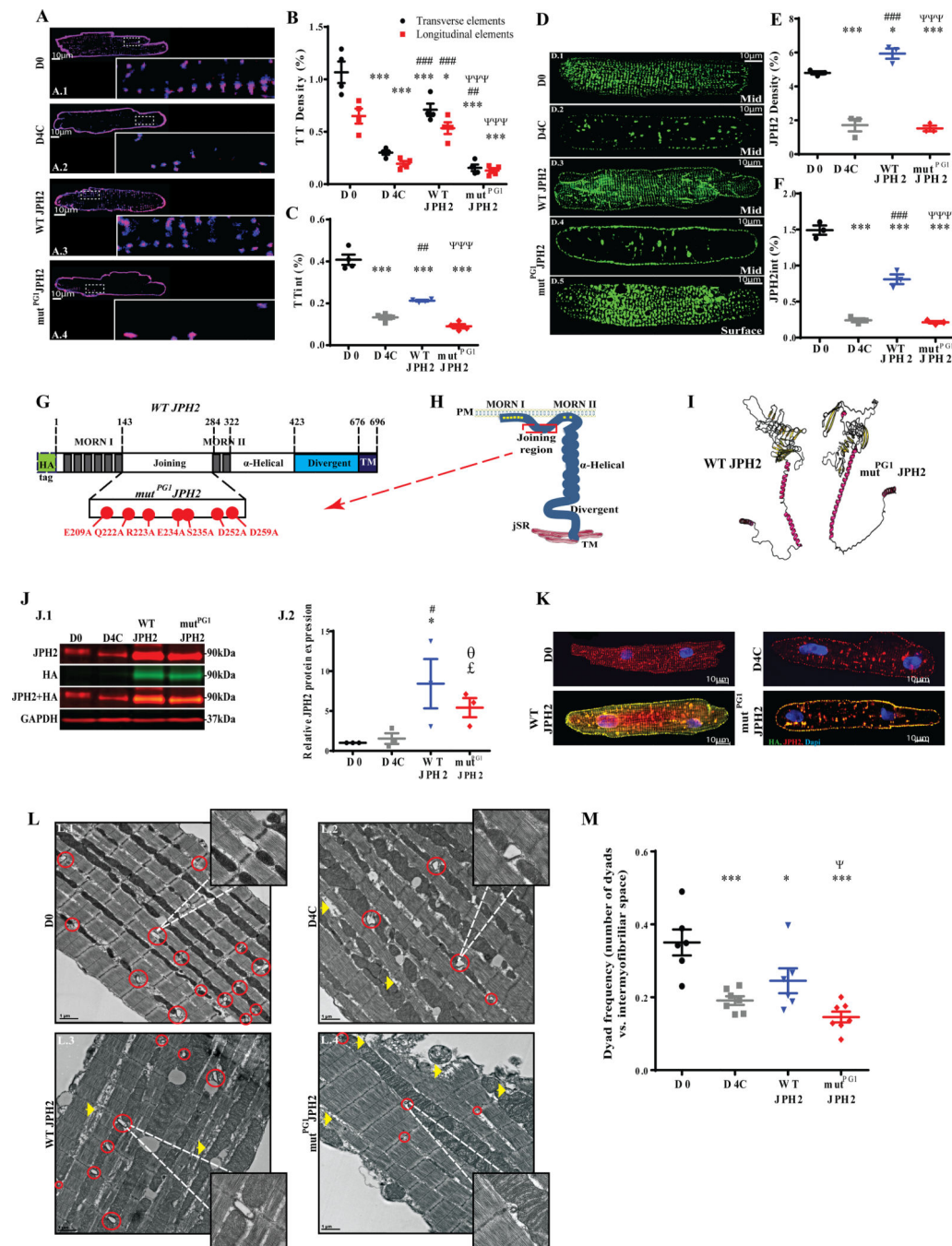
Figure 2. JPH2 and T-tubular remodeling in cultured AFVMs with and without Adenoviral expression of human WT-JPH2 and mut[PG1]JPH2 constructs in cultured AFVMs.

(**A**) Distribution of T-tubules detected by Di-8-ANEPPS staining in freshly isolated AFVMs at day 0 (D0), after 4 days of culture in control AFVMs (D4C), in AFVMs after 4 days in culture overexpressing Ad-WT-JPH2 (WT-JPH2) and in AFVMs after 4 days in culture overexpressing Ad-myt[PG1]JPH2 (mut[PG1]JPH2). WT-JPH2 overexpression preserved T-tubules while overexpression of mut[PG1]JPH2 did not preserve T-tubules in cultured AFVMs. Scale 10μm. The entire area of the cell was selected to measure t-tubule density and

integrity. **(B)** T-tubular transverse and longitudinal densities. Data are shown as means ± SEM, N=4 isolations, for D0 n=15 cells and for the rest of the groups n=20 cells. For transverse elements comparison: ***P=8.45×10^{-9} D4C vs. D0, ***P=6.53×10^{-6} WT vs. D0, ***P=1.8×10^{-9} mut^{PG1}JPH2 vs. D0; ###P=2.09×10^{-6} WT-JPH2 vs. D4C and ##P=0.0068 mut^{PG1}JPH2 vs. D4C; ¥¥¥P=1.48×10^{-7} mut^{PG1}JPH2 vs. WT-JPH2. For longitudinal elements comparison: ***P=8.4×10^{-7} D4C vs. D0, *P=0.0288 WT-JPH2 vs. D0, ***P=2.6×10^{-7} mut^{PG1}JPH2 vs. D0; ###P=1.03×10^{-5} WT-JPH2 vs. D4C; ¥¥¥P=2.28×10^{-6} mut^{PG1}JPH2 vs. WT-JPH2. 2-way ANOVA multiple comparisons test was applied after making all six possible comparisons. Adjusted p-values were obtained after Sidak's correction. **(C)** Global T-tubular integrity. Data are shown as means ± SEM, N=4 isolations, for D0 n=15 cells and for the rest of the groups n=20 cells. ***P=6.19×10^{-8} D4C vs. D0, ***P=2.67×10^{-6} WT JPH2 vs. D0, ***P=1.2×10^{-8} mut^{PG1}JPH2 vs. D0; ##P=0.0094 WT-JPH2 vs. D4C and ¥¥¥P=0.0003 mut^{PG1}JPH2 vs. WT-JPH2. One-way ANOVA multiple comparisons test was applied after making all six possible comparisons. Adjusted p-values were obtained after Tukey correction. **(D)** Representative images of JPH2 staining in AFVMs at D0, control cells at D4, and AFVMs overexpressed with either Ad-WT-JPH2 or Ad-mut^{PG1}JPH2. I.1 – I.4 images represent mid-section of the cells obtained via Z-stack confocal scanning. D.5 image represents the surface of the cell. Scale 10μm. **(E)** Calculated JPH2 global density. Data is shown as means ± SEM, N=3 isolations, for D0 n=10 cells and for the rest of the groups n =15 cells. ***P=0.0001 D4C vs. D0, *P=0.05 WT JPH2 vs. D0, ***P=7.96×10^{-5} mut^{PG1}JPH2 vs. D0; ###P=1.22×10^{-5} WT-JPH2 vs. D4C and ¥¥¥P=8.66×10^{-6} mut^{PG1}JPH2 vs. WT-JPH2. One-way ANOVA multiple comparisons test was applied after making all six possible comparisons. Adjusted p-values were obtained after Tukey correction. **(F)** JPH2 global integrity in the mid-section of the cell. Data is shown as means ± SEM, N=3 isolations, n=10 cells and for the rest of the groups n =15 cells. ***P=4.22×10^{-7} D4C vs. D0, ***P=4.54×10^{-5} WT-JPH2 vs. D0, ***P=3.47×10^{-7} mut^{PG1}JPH2 vs. D0. ###P=0.0002 WT-JPH2 vs. D4C and ¥¥¥P=0.0001 mut^{PG1}JPH2 vs. WT-JPH2. One-way ANOVA multiple comparisons test was applied after making all six possible comparisons. Adjusted p-values were obtained after Tukey correction. **(G)** Protein topology of human JPH2 isoform (1–696 amino acids) that was cloned into Adenovirus WT-JPH2 contains an HA tag on the N-terminus, MORN motifs, joining region, α-helical domain, divergent and transmembranal (TM) domains. The zoomed joining region shows the seven-point mutations that were modified in Adenovirus mut^{PG1}JPH2 are shown. **(H)** Overview of human JPH2 localized in the dyad of cardiomyocyte. The illustration depicts the structure of JPH2 domains. The region highlighted in the red box is the Joining region that was mutated in Ad-mut^{PG1}JPH2. **(I)** Template-based tertiary structure modeling of HA tagged WT-JPH2 (P-value 1.37×10^{-05}) and mut^{PG1}JPH2 (P-value 2.29×10^{-05}) proteins via RaptorX. **(J.1)** Representative Western blot and **(J.2)** Densitometry of JPH2 protein expression normalized to GAPDH. Data represented as means ± SEM, N=3. *P=0.0269 WT-JPH2 vs. D0, #P=0.05 WT-JPH2 vs. D4C. £P=0.0578 mut^{PG1}JPH2 vs. D0 and ℮P=0.1 mut^{PG1}JPH2 vs. D4C. Non-parametric Friedman multiple comparisons test with preselected pairs (D0 vs. WT and mutant JPH2 and D4C vs. WT and mutant JPH2) was applied. Adjusted p-values were obtained after Dunn's correction. **(K)** Immunofluorescence staining of JPH2 and HA in freshly (D0) isolated AFVMs, control cultured AFVMs for 4 days (D4C), Ad-WT-JPH2 with HA tag transduced AFVMs and Ad-mut^{PG1}JPH2 with HA tag

transduced AFVMs. Scale 10μm. **(L)** mut^{PG1}JPH2 expression induces downregulation of dyad distribution. Z-line organization and distribution of the dyads were evaluated in D0/D4C/WT-JPH2/mut^{PG1}JPH2 AFVMs. Dyads are indicated in red circles. Myofilament degradation is indicated via yellow arrows. Scale 1μm. **(M)** Frequency of dyads quantified as the number of dyads per number of intermyofibrillar spaces. Data are shown means ± SEM, N= 6–7 randomly analyzed cells per group, n=15 totals dyads analyzed per group. ***P=0.0009 D4C vs. D0, *P=0.0401 WT-JPH2 vs. D0 and ***P=4.16×10^{-5} mut^{PG1}JPH2 vs. D0; ¥P=0.0449 mut^{PG1}JPH2 relative to WT-JPH2. One-way ANOVA multiple comparisons test was applied after making all six possible comparisons. Adjusted p-values were obtained after Tukey correction.
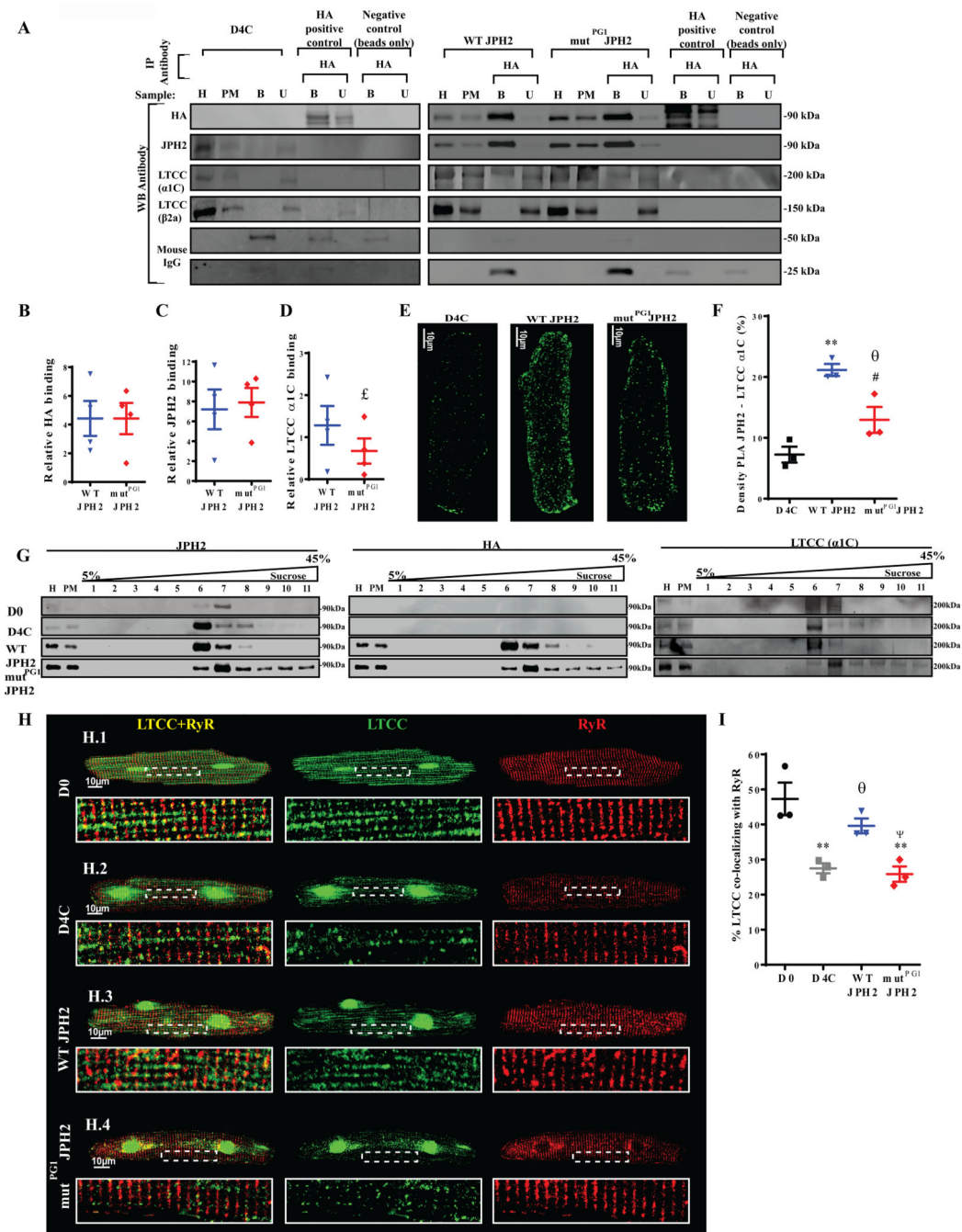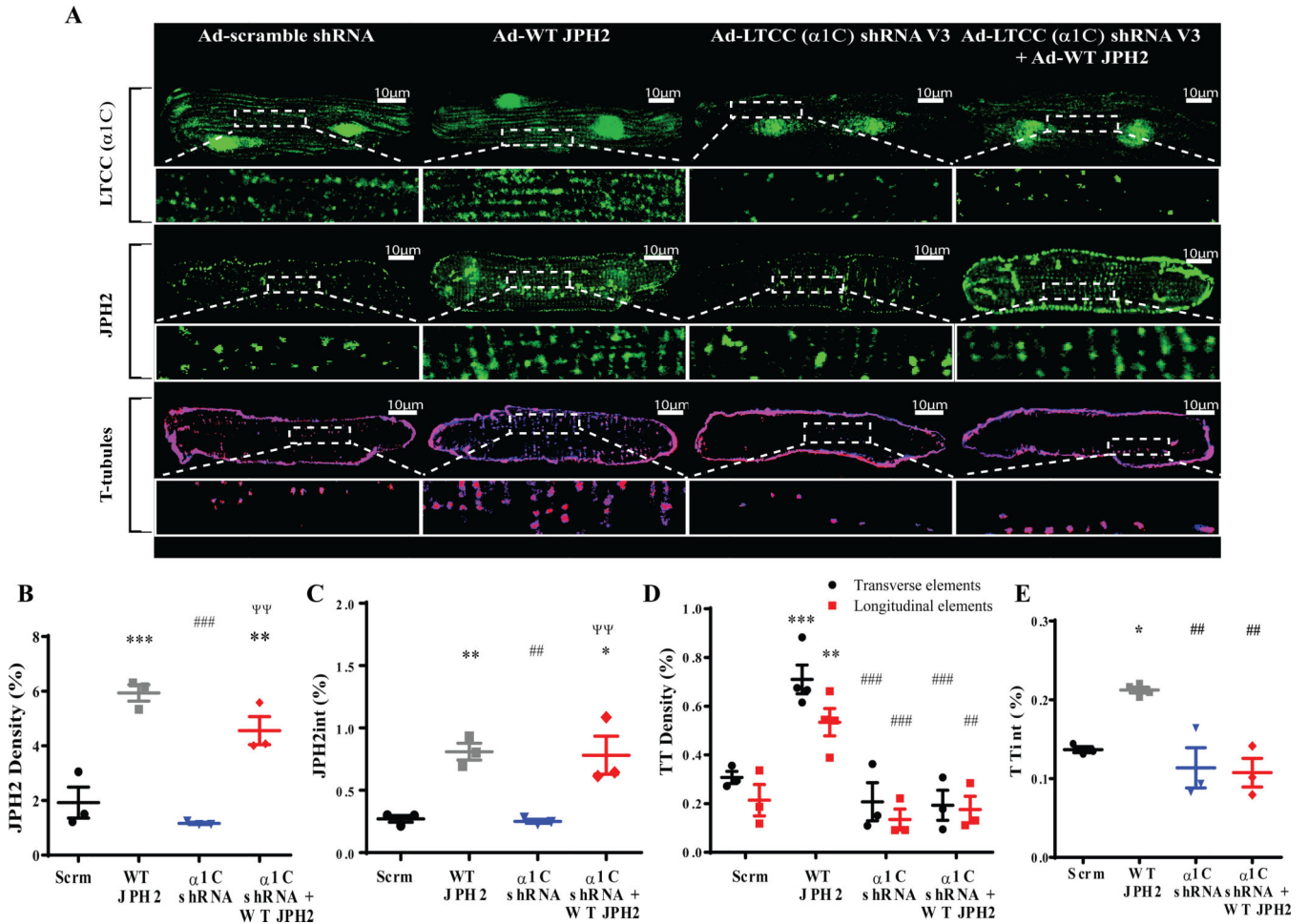
Figure 3. The Joining region in JPH2 interacts with LTCC α1C and regulates membrane microdomain distribution of LTCCs.

(**A**) HA-tag co-immunoprecipitation (Co-IP) was performed on purified PM from AFVMs that were expressing either Ad-WT-JPH2 or Ad-mut^PG1JPH2. HA, JPH2, LTCC α1C and LTCC β2a were detected in whole cell homogenate (H), PM, HA bound (B) fraction and unbound (U) fraction. Co-IP was performed using magnetic beads conjugated with HA mouse antibody. Therefore, mouse IgG expression was tested. HA positive control was Escherichia coli extract containing HA tagged GST-PI3K-SH2 domain. (**B**) Quantification

of co-immunoprecipitation experiments of HA pull-down, **(C)** JPH2 Co-IP and **(D)** LTCC α1C Co-IP between WT-JPH2 and mut^{PG1}JPH2 overexpressing AFVMs. Each bound fraction was normalized to its PM input. Data are means ± SEM of N=3 independent Co-IP experiments. Non-parametric Wilcoxon test was applied. $^£$P=0.0625. **(E)** Proximity ligation (PLA) assay was performed on AFVMs infected with Ad-WT-JPH2, or with Ad-mut^{PG1}JPH2 to detect protein-protein interaction between JPH2-LTCC α1C subunit. **(F)** PLA density was measured as the fraction of an area covered by the fluorescence signal. Average values were calculated from at least n=5 cells per isolation. Data are shown as mean ± SEM, N=3 isolations/experiments. **P=0.0018 WT-JPH2 vs. D4C, ^{e}P=0.0902 mut^{PG1}JPH2 vs. D4C and $^\#$P=0.0226 mut^{PG1}JPH2 vs. WT-JPH2. One-way ANOVA multiple comparisons test was applied after making all three possible comparisons. Adjusted p-values were obtained after Tukey correction. **(G)** Representative Western blots of JPH2 and LTCC (α1C) across sucrose density gradient fractions (F1–F11) of D0, D4C, WT-JPH2 and mut^{PG1}JPH2 overexpressed AFVMs. **(H)** AFVMs at D0 (panel H.1), D4C (panel H.2), overexpressed with WT-JPH2 (panel H.3) and overexpressed with mut^{PG1}JPH2 (panel H.4) were immunostained for RyR (red channel – right column) and LTCC α1C subunit (green channel – middle column). The overlay of green and red channels is depicted in the left column. **(I)** Distance based co-localization percentage of LTCC α1C with RyR. The entire cell surface was analyzed for co-localization excluding the nuclei. Data are shown as mean ± SEM from N=3 isolations/experiments. n=15 cells per experiment were analyzed in each group. **P=0.0054 D4C vs. D0, **P=0.0033 mut^{PG1}JPH2 vs. D0, ^{e}P=0.0681 WT-JPH2 vs. D4C and $^¥$P=0.0386 mut^{PG1}JPH2 vs. WT-JPH2. One-way ANOVA multiple comparisons test was applied after making all six possible comparisons. Adjusted p-values were obtained after Tukey correction.

Figure 4. LTCC and JPH2 jointly stabilize T-tubules.
(A) AFVMs were transduced with Ad-scrambled shRNA, Ad-WT-JPH2, Ad-LTCC (α1C) shRNA-V3 and combination of Ad-LTCC (α1C) shRNA-V3 + Ad-WT-JPH2. Immunostaining for LTCC α1C is shown in the upper panel, confirming knock down of LTCC. JPH2 staining is shown in the middle panel and di-8-ANPPES T-tubular stain is presented in the lower panel. **(B)** Quantification of JPH2 density. Data are shown means ± SEM, N=3 isolations, n=10 cells per group. ***P=0.0006 WT-JPH2 vs. Scrm, **P=0.0084 α1C shRNA+WT-JPH2 vs. WT-JPH2, ###P=0.0002 α1C shRNA vs. WT-JPH2, ¥¥P=0.0018 α1C shRNA+WT-JPH2 vs. α1C shRNA. One-way ANOVA multiple comparisons test was applied after making all six possible comparisons. Adjusted p-values were obtained after Tukey correction. **(C)** JPH2 staining integrity analysis. Data are shown means ± SEM, N=3 isolations, n=10 cells per group. **P=0.0087 WT-JPH2 vs. Scrm, *P=0.0119 α1C shRNA +WT-JPH2 vs. WT-JPH2, ##P=0.0071 α1C shRNA vs. WT-JPH2 and ¥¥P=0.0096 α1C shRNA+WT-JPH2 vs. α1C shRNA. One-way ANOVA multiple comparisons test was applied after making all six possible comparisons. Adjusted p-values were obtained after Tukey correction. **(D)** T-tubular density analysis. Data are shown means ± SEM, N=3 isolations, n=10 cells per group. For transverse comparisons: ***P=0.0005 WT-JPH2 vs. Scrm, ###P=3.85×10^{-5} α1C shRNA vs. WT-JPH2, ###P=2.68×10^{-5} α1C shRNA+WT-JPH2

vs. WT-JPH2. For longitudinal comparisons: [**]P=0.005 WT-JPH2 vs. Scrm, [###]P=0.0006 α1C shRNA vs. WT-JPH2 and [##]P=0.0017 α1C shRNA+WT-JPH2 vs. WT-JPH2. 2-way ANOVA multiple comparisons test was applied after making all six possible comparisons. Adjusted p-values were obtained after Sidak's correction. **(E)** T-tubular integrity analysis. Data are shown means ± SEM, N=3 isolations, n=10 cells per group. For transverse comparisons: *P=0.0183 WT-JPH2 vs. Scrm, [##]P=0.0036 α1C shRNA vs. WT-JPH2 and [##]P=0.0024 α1C shRNA+WT-JPH2 vs. WT-JPH2. One-way ANOVA multiple comparisons test was applied after making all six possible comparisons. Adjusted p-values were obtained after Tukey correction.
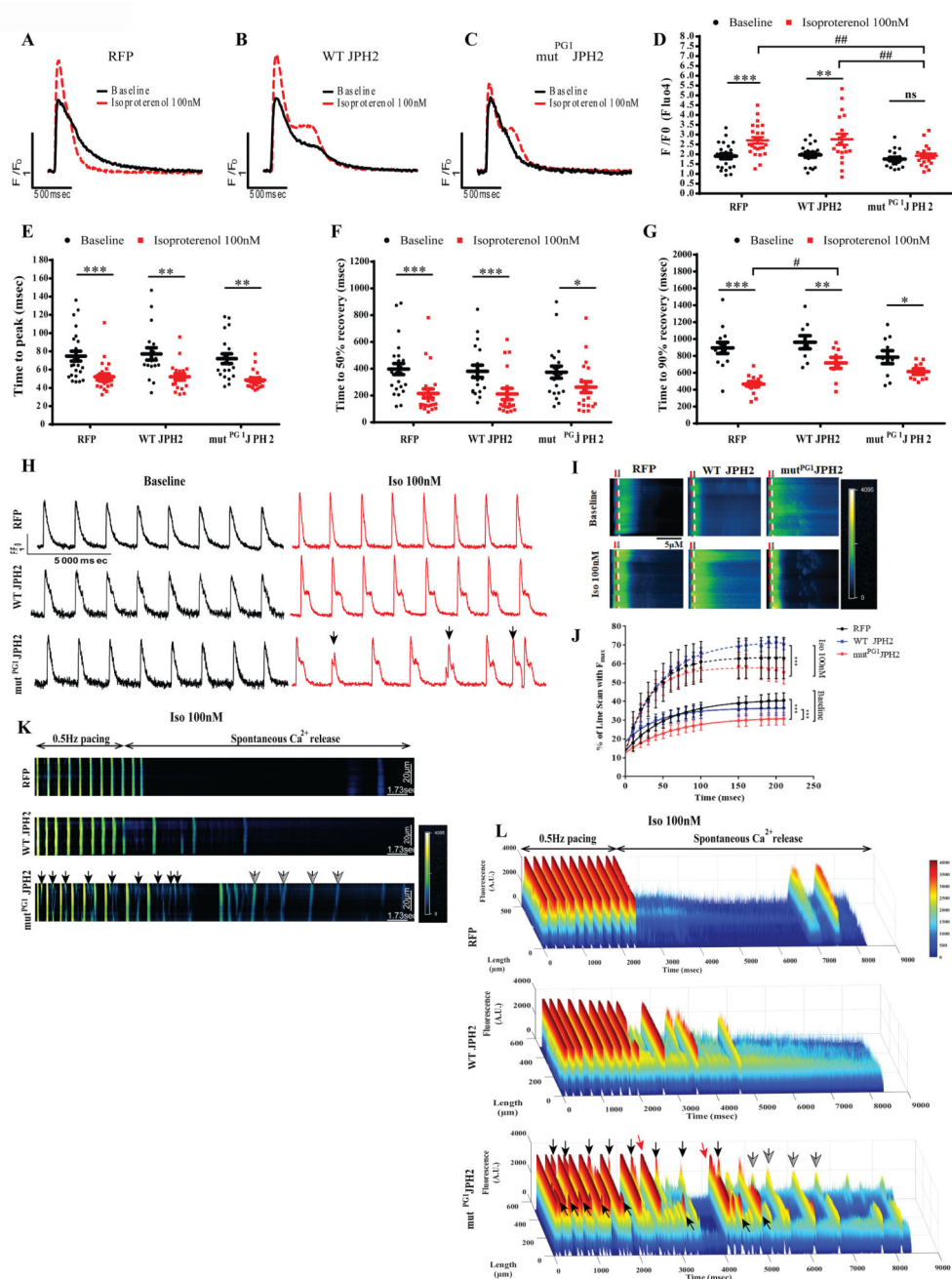
Figure 5. Mutation of the Joining region in JPH2 alters Ca^{2+} signaling in AFVMs after β-adrenergic stimulation.

Representative recordings of intracellular Ca^{2+} transients (Fluo-4) in AFVMs overexpressed with **(A)** Ad-RFP, **(B)** Ad-WT-JPH2, **(C)** Ad-mut^{PG1}JPH2 paced at 0.5Hz with or without isoproterenol (Iso 100nM). **(D)** Ca^{2+} transient peak amplitude. Data are shown as means ± SEM collected from isolated AFVMs (biological replicates) n=20 cells per group, N=3 heart isolations. ***P=0.0008 RFP Iso vs. baseline, **P=0.0038 WT JPH2 Iso vs. baseline, $^{\#\#}$P=0.0018 mut^{PG1}JPH2 vs. RFP after Iso effect and $^{\#\#}$P=0.0016 mut^{PG1}JPH2 vs. WT JPH2

after Iso effect. 2-way ANOVA multiple comparisons test was applied after making all six possible comparisons. Adjusted p-values were obtained after Sidak's correction. **(E)** Ca^{2+} time to peak amplitude. ***P=0.001 RFP Iso vs. baseline, **P=0.0014 WT JPH2 Iso vs. baseline and **P=0.002 mut^{PG1}JPH2 Iso vs. baseline. 2-way ANOVA multiple comparisons test was applied after making all six possible comparisons. Adjusted p-values were obtained after Sidak's correction. **(F)** Ca^{2+} time to 50% decay. ***P=4.37×10^{-6} RFP Iso vs. baseline, ***P=0.0002 WT JPH2 Iso vs. baseline and *P=0.0121 mut^{PG1}JPH2 Iso vs. baseline. 2-way ANOVA multiple comparisons test was applied after making all six possible comparisons. Adjusted p-values were obtained after Sidak's correction. **(G)** Time to 90% decay. ***P=7.37×10^{-9} RFP Iso vs. baseline, **P=0.0019 WT JPH2 Iso vs. baseline and *P=0.0256 mut^{PG1}JPH2 Iso vs. baseline. 2-way ANOVA multiple comparisons test was applied after making all six possible comparisons. Adjusted p-values were obtained after Sidak's correction. **(H)** Representative traces of paced AFVMs expressing RFP/WT-JPH2/ mut^{PG1}JPH2 with and without iso 100nM. Cells were paced at 0.5Hz. Spontaneous Ca^{2+} oscillations are indicated via black arrows. **(I)** Ca^{2+} release synchrony obtained via confocal line scanning of RFP/WT- JPH2/ mut^{PG1}JPH2 AFVMs. Cells were paced at 0.5Hz with or without Iso 100nM. Spatial profiles are highlighted at 10msec (red dotted line) and 40msec (white dotted line). **(J)** Percentage of line scan with an index of F/F_{max} representing spatial synchrony of Ca^{2+} release. n=10 cells per group. ***P=1.03×10^{-9} RFP vs. mut^{PG1}JPH2 and ***P=3.13×10^{-8} WT JPH2 vs. mut^{PG1}JPH2 in comparison of non-linear fits using extra sum-of-squares F test at baseline conditions. ***P=2.35×10^{-6} WT JPH2 vs. mut^{PG1}JPH2 in comparison of non-linear fits using extra sum-of-squares F test after Iso 100nM treatment. **(K)** Representative line scan recordings of AVFMs expressing RFP/WT-JPH2/ mut^{PG1}JPH2, treated with 100nM Iso and paced at 0.5Hz. Asynchronous Ca^{2+} release during pacing is indicated via black arrows. Ca^{2+} alternans are indicated via grey arrows. **(L)** Representative 3D-reconstruction of representative line-scan recordings determine the characteristics of spatial Ca^{2+} waves spreading in space and time. Red arrows indicate spontaneous Ca^{2+} release.
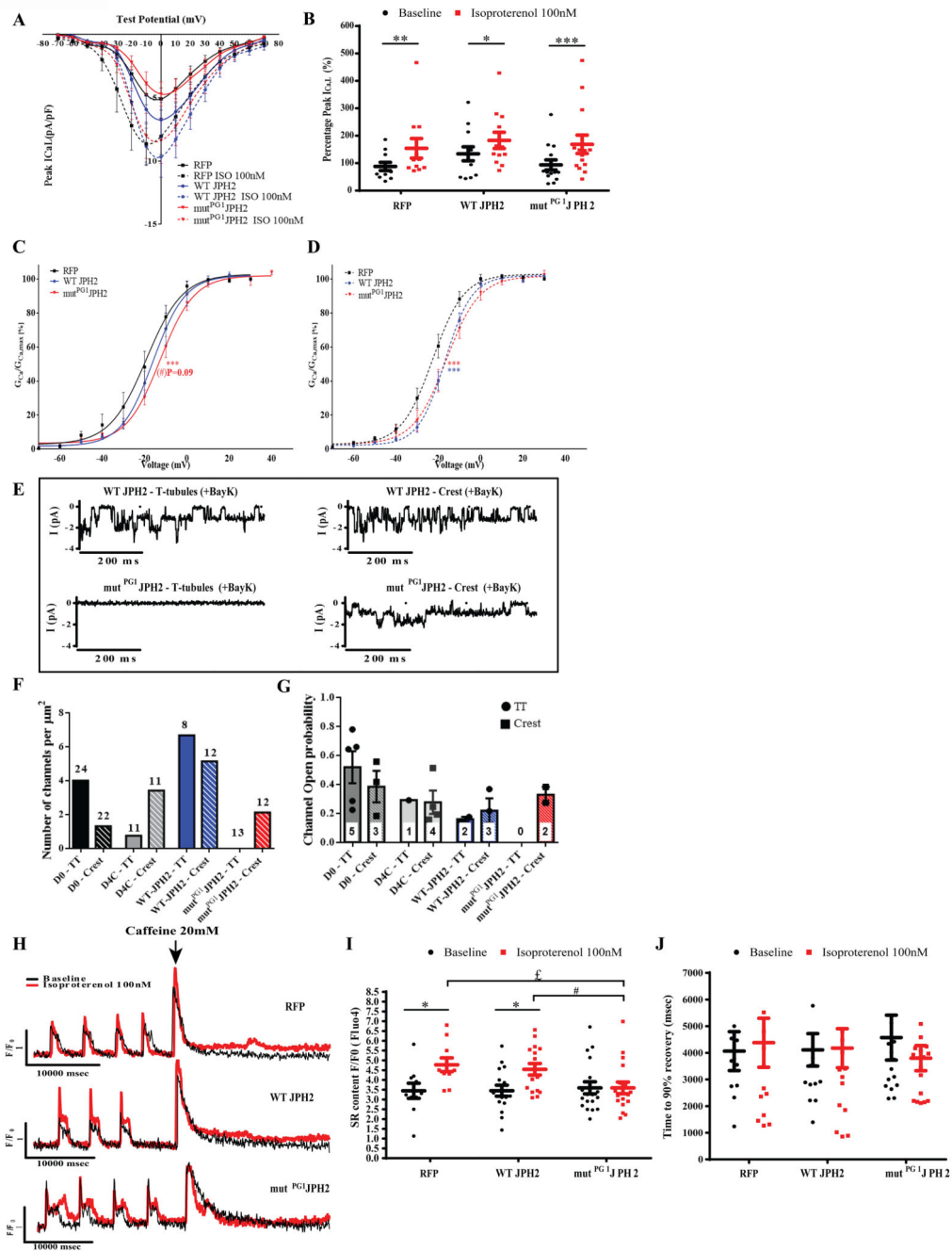
Figure 6. Abnormal LTCC localization to the crest with modified voltage dependence of activation in mut^PG1^JPH2 AFVMs.

(**A**) $I_{Ca,L}$-voltage relationships in RFP/WT-JPH2/ mut^PG1^JPH2 overexpressed AFVMs with or without Iso 100nM. N=3 isolations. For RFP n=11 and for WT and mutant JPH2 n=14 cells per group. (**B**) Peak amplitude of Ca^{2+} current through LTCC. Data are shown as means ± SEM collected from isolated AFVMs (biological replicates), RFP n=11 and for WT and mutant JPH2 n=14 cells per group, N=3 heart isolations. **P=0.004 RFP Iso vs. baseline, *P=0.031 WT JPH2 Iso vs. baseline and ***P=0.0002 mut^PG1^JPH2 Iso vs.

baseline. 2-way ANOVA multiple comparisons test was applied after making all six possible comparisons. Adjusted p-values were obtained after Sidak's correction. Voltage dependence of $I_{Ca,L}$ activation in RFP/WT-JPH2/ mut^{PG1}JPH2 overexpressed AFVMs were fit with Boltzmann Equation $G/G_{max}=1/[1+exp(V_{0.5}-V)/k]$ in baseline **(C)** and in response to Iso 100nM **(D)**. N=3 isolations, for RFP n=11 and for WT and mutant JPH2 n=14 cells per group. In figure C: ***P=0.001mut^{PG1}JPH2 vs. RFP and $^{(\#)}$P=0.0909 mut^{PG1}JPH2 vs. WT JPH2 using comparison of Boltzmann sigmoidal fits (Extra sum-of-squares F test). In figure D: ***P=9.61×10^{-10} WT JPH2 vs. RFP and ***P=4.34×10^{-6} mut^{PG1}JPH2 vs. RFP using comparison of Boltzmann sigmoidal fits (Extra sum-of-squares F test). **(E)** Single LTCC activity was recorded in T-tubules or non-tubular areas of the surface membrane (Crest) using super-resolution scanning patch clamp in the presence of the LTCC agonist BayK8644 (5μM in the pipette). Examples of original recordings from a holding potential of −96.7mV, channels were activated by a step to −6.7mV. **(F)** Channel density calculated per μm^2. The number indicated for each column is the total number of patches. **(G)** Channel open probability at −6.7 mV. The number indicated for each column is number of patches with one or more Ca^{2+} channel(s). 2-way ANOVA multiple comparisons test was applied after making all six possible comparisons. Adjusted p-values were obtained after Sidak's correction. **(H)** Representative traces of Ca^{2+} transient amplitudes and total SR content indicated by the amplitude of caffeine induced SR Ca^{2+} release in paced AFVMs. **(I)** SR Ca^{2+} release peak amplitude. Data are shown as means ± SEM collected from isolated AFVMs (biological replicates) n=15 cells per group, N=3 heart isolations. *P=0.0433 RFP Iso vs. baseline, *P=0.0338 WT JPH2 Iso vs. baseline, $^{\#}$P=0.0403 mut^{PG1}JPH2 vs. RFP after Iso effect and P=0.0637 mut^{PG1}JPH2 vs. WT JPH2 after Iso effect. $^{£}$P=0.0637 mut^{PG1}JPH2 vs. WT-JPH2 after Iso effect. 2-way ANOVA multiple comparisons test was applied after making all six possible comparisons. Adjusted p-valu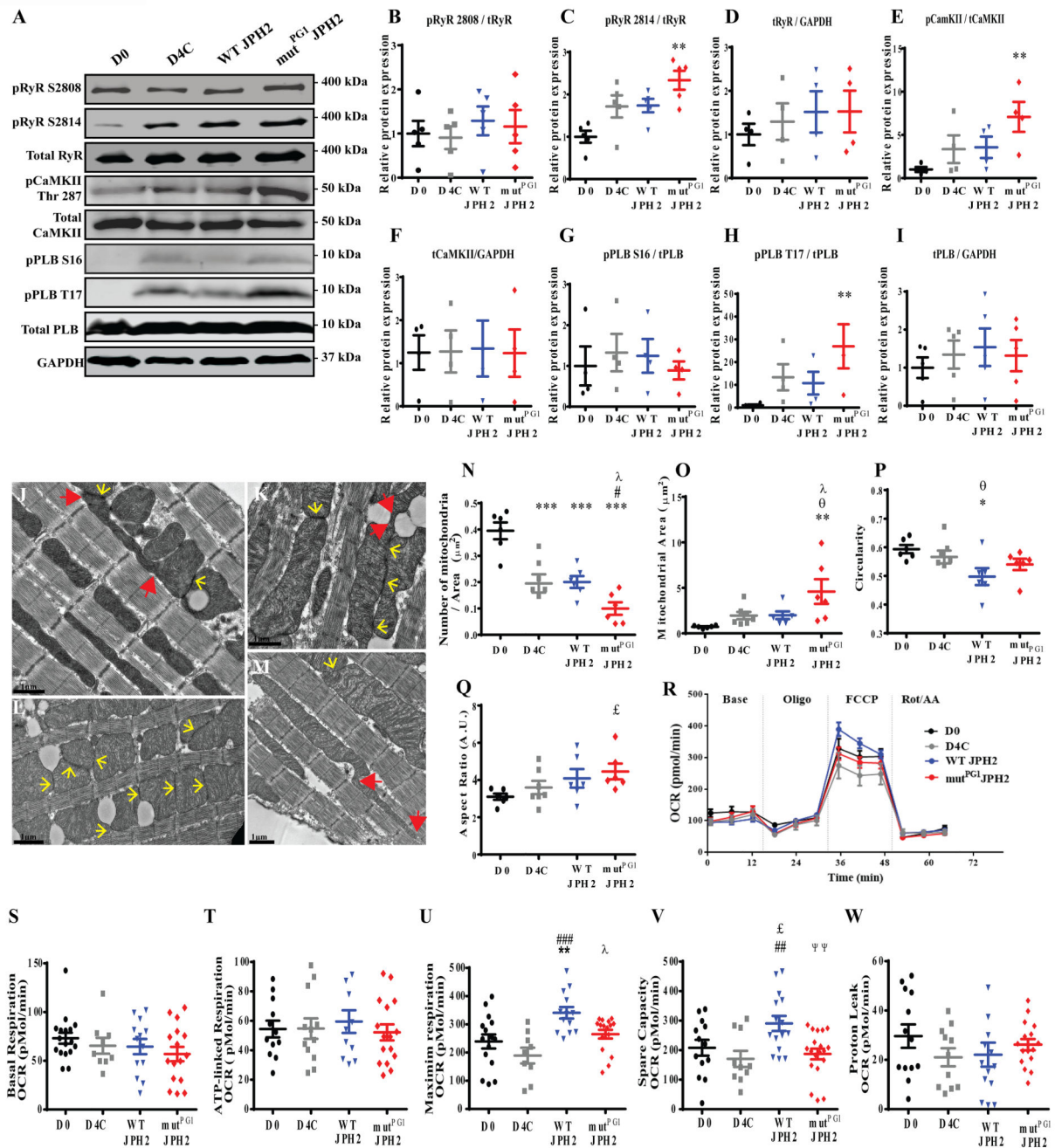es were obtained after Sidak's correction. **(J)** Time to 90% recovery from Ca^{2+} peak after caffeine addition. Data are presented as mean ± SEM. N=3 isolations, n= 15. 2-way ANOVA multiple comparisons test was applied after making all six possible comparisons. Adjusted p-values were obtained after Sidak's correction.

Figure 7. Global effect of WT-JPH2 and mut^PG1^JPH2 overexpression on Ca^{2+} handling proteins and mitochondrial disposition, morphogenesis and bioenergetics in AFVMs.
(**A**) Representative Western blot of EC coupling and Ca^{2+} handling proteins: RyR (basal and phosphorylated states), PLB (total and phosphorylated states) and CaMKII (basal and phosphorylated states). Whole-cell lysates from freshly isolated AFVMs (D0), control cultured AFVMs for 4 days (D4C), Ad-WT-JPH2 or Ad-mut^PG1^JPH2 overexpressed AFVMs 4 days in culture were tested for protein expression levels. (**B-I**) Average quantified values expressed relative to D0 AFVMs. Tested protein levels were normalized to GAPDH

loading control. Phosphorylated protein expression was normalized to total protein expression. Data presented as means ± SEM, N=3–5 experiments. Significant p-values are shown as follows: **[B]** Non-parametric Friedman multiple comparisons test was applied after making three possible comparisons between mut[PG1]JPH2 to D0/D4C/WT-JPH2. Adjusted p-values were obtained after Dunn's correction. No significance was detected. **[C]** **P=0.0018 mut[PG1]JPH2 vs. D0. Non-parametric Friedman multiple comparisons test was applied after making three possible comparisons between mut[PG1]JPH2 to D0/D4C/WT-JPH2. Adjusted p-values were obtained after Dunn's correction. **[D]** Non-parametric Friedman multiple comparisons test was applied after making three possible comparisons between mut[PG1]JPH2 to D0/D4C/WT-JPH2. Adjusted p-values were obtained after Dunn's correction. No significance was detected. **[E]** **P=0.0078 mut[PG1]JPH2 vs. D0. Non-parametric Friedman multiple comparisons test was applied after making three possible comparisons between mut[PG1]JPH2 to D0/D4C/WT-JPH2. Adjusted p-values were obtained after Dunn's correction. **[F-G]** Non-parametric Friedman multiple comparisons test was applied after making three possible comparisons between mut[PG1]JPH2 to D0/D4C/WT-JPH2. Adjusted p-values were obtained after Dunn's correction. No significance was detected. **[H]** **P=0.0031 mut[PG1]JPH2 vs. D0. Non-parametric Friedman multiple comparisons test was applied after making three possible comparisons between mut[PG1]JPH2 to D0/D4C/WT-JPH2. Adjusted p-values were obtained after Dunn's correction. **[I]** Non-parametric Friedman multiple comparisons test was applied after making three possible comparisons between mut[PG1]JPH2 to D0/D4C/WT-JPH2. Adjusted p-values were obtained after Dunn's correction. No significance was detected. Ultrastructure of cardiac mitochondria in **(J)** D0 cardiomyocytes, **(K)** D4C cardiomyocytes, **(L)** WT-JPH2 overexpressed cardiomyocytes and **(M)** mut[PG1]JPH2 overexpressed cardiomyocytes. Physical contact between two adjacent mitochondria termed as "kissing events" is indicated via yellow arrows. Sites of longitudinally oriented nanotunnels are indicated between the red arrows. Long distance nanotunnel shown in D0 myocyte has length of 2.6μm and diameter of 194nm. Short distance nanotunnel represented in D4C myocyte has length of 567nm and diameter of 0.121nm. Long distance nanotunnel indicated in mut[PG1]JPH2 myocytes has length of 4.05μm and diameter of 306nm. **(N)** Quantification of number of mitochondria per cellular area. Data are presented as means ± SEM, N=6. ***P=0.0010 D4C vs. D0, ***P=0.0003 WT-JPH2 vs. D0, ***$P=1.26\times10^{-6}$ mut[PG1]JPH2 vs. D0. #P=0.0269 mut[PG1]JPH2 vs. D4C and $^{\lambda}$P=0.0714 mut[PG1]JPH2 vs. WT-JPH2. One-way ANOVA multiple comparisons test was applied after making all six possible comparisons. Adjusted p-values were obtained after Tukey correction. **(O)** Measurement of mitochondrial area. Data are presented as means ± SEM, N=6. **P=0.0061 mut[PG1]JPH2 vs. D0, ᵉP=0.0668 mut[PG1]JPH2 vs. D4C and $^{\lambda}$P=0.0878 mut[PG1]JPH2 vs. WT-JPH2. One-way ANOVA multiple comparisons test was applied after making all six possible comparisons. Adjusted p-values were obtained after Tukey correction. **(P)** Quantification of mitochondrial shape including circularity. Data are presented as means ± SEM, N=6. *P=0.0249 WT-JPH2 vs. D0 and ᵉP=0.0596 WT-JPH2 vs. D4C. One-way ANOVA multiple comparisons test was applied after making all six possible comparisons. Adjusted p-values were obtained after Tukey correction. **(Q)** Aspect ratio. Data are presented as means ± SEM, N=6. £P=0.0928 mut[PG1]JPH2 vs. D0. One-way ANOVA multiple comparisons test was applied after making all six possible comparisons. Adjusted p-values were obtained after Tukey correction. **(R)** Seahorse analysis of

mitochondrial oxygen consumption rates (OCR) in AFVMs. n = 15 for D0 and n=20 for D4C/WT JPH2/mut^{PG1}JPH2 conditions from N=3 AFVMs isolations. **(S)** Basal OCR. **(T)** ATP-linked respiration after addition of ATP synthase inhibitor, oligomycin. **(U)** Maximal respiration after addition of protonophore, FCCP. Data are presented as means ± SEM, **P=0.0075 WT-JPH2 vs. D0, ###P=0.0003 WT-JPH2 vs. D4C and $^{\lambda}$P=0.0628 WT-JPH2 vs. mut^{PG1}JPH2. **(V)** Spare respiratory capacity (max − basal). Data are presented as means ± SEM, $^{£}$P=0.0850 WT-JPH2 vs. D0, ##P=0.0098 WT-JPH2 vs. D4C and ¥¥P=0.0083 WT-JPH2 vs. mut^{PG1}JPH2. **(W)** Proton leak (post-oligomycin OCR − non-mitochondrial OCR). One-way ANOVA multiple comparisons test was applied after making all six possible comparisons. Adjusted p-values were obtained after Tukey correction.
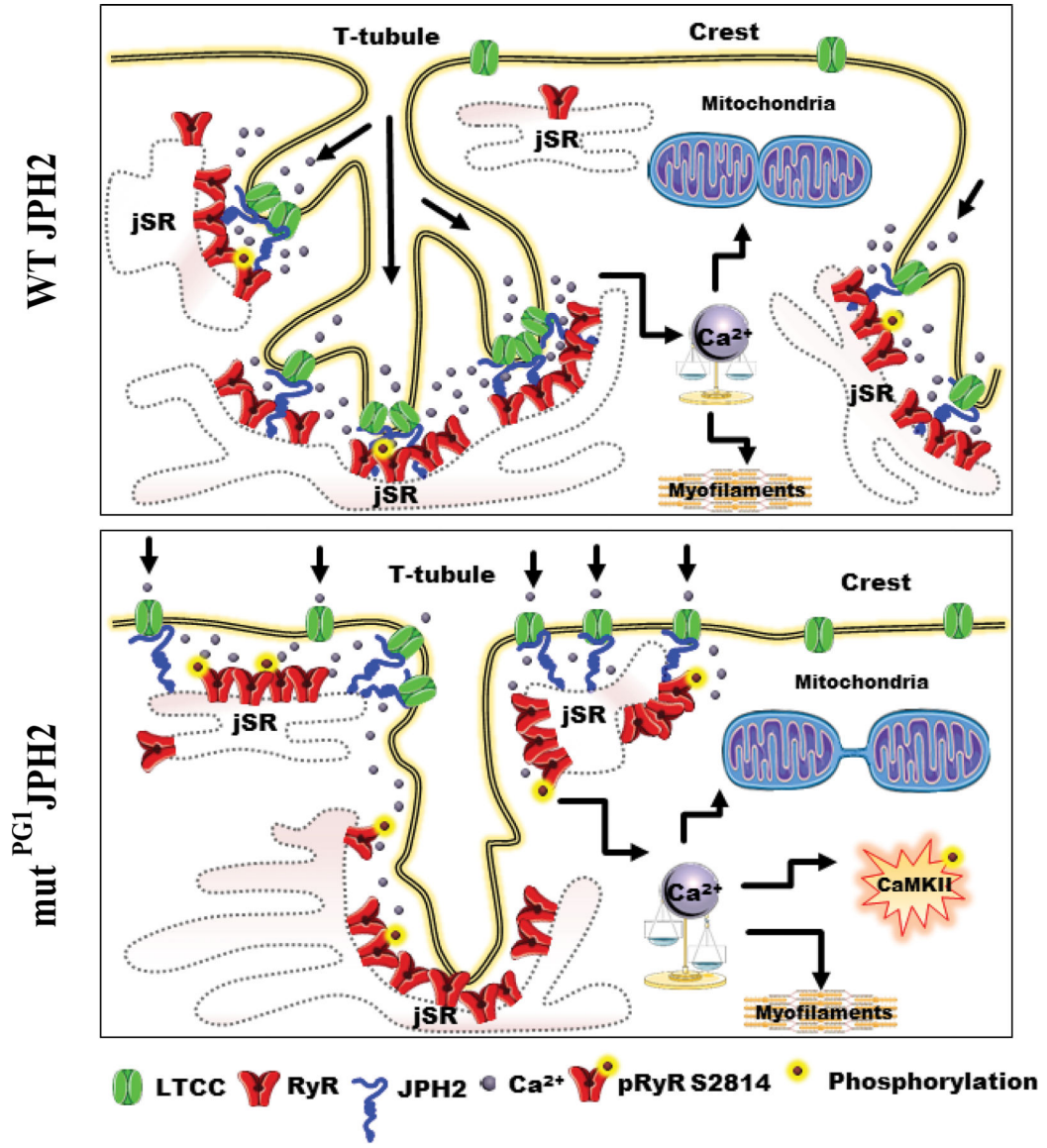
Figure 8. Representative illustration of the LTCC-JPH2 interaction via the Joining region in cardiomyocyte.

[Top] In WT-JPH2 expressing cardiomyocytes, LTCCs are recruited to the T-tubules and interact with the Joining region in JPH2. LTCCs are localized in spatial proximity to the juxtaposed RyRs forming a dyad complex that enables efficient EC coupling. These myocytes exhibit balanced Ca^{2+} dynamics and tight junctions between mitochondria. **[Bottom]** In mut^{PG1}JPH2 expressing cardiomyocytes, the T-tubular network becomes degraded and there are fewer dyads. LTCCs translocate to the crest, leaving "orphaned" RyRs at the jSR. LTCCs have reduced interaction with JPH2, whereas the remaining LTCC-JPH2 interactions take place at the crest. Ca^{2+} regulation in these myocytes is abnormal and prone to spontaneous SR Ca^{2+} release and mitochondria appear to communicate through long-distance tunnels.